Carbohydrate Polymer Technologies and Applications 9 (2025) 100739

Contents lists available at ScienceDirect

Carbohydrate Polymer Technologies and Applications

journal homepage: www.sciencedirect.com/journal/carbohydrate-polymer-technologies-and-applications

Impacts of cycles of a novel low-pressure homogenization process on cellulose nanofibrils (CNF) as a sustainable packaging film material

Belladini Lovely [a], Young-Teck Kim [a,*], Haibo Huang [b], Audrey Zink-Sharp [a], Maren Roman [a]

[a] Department of Sustainable Biomaterials, Virginia Tech, Blacksburg, VA 24061, USA
[b] Department of Food Science and Technology, Virginia Tech, Blacksburg, VA 24061, USA

ARTICLE INFO

Keywords:
Cellulose nanofibrils (CNF)
Homogenization
Number of cycles or passes
Mechanical properties
Oxygen permeability

ABSTRACT

Cellulose nanofibrils (CNF) have been among the most researched materials for their myriad advantages, yet are still facing challenges toward advanced developments due to their natural hydrophilicity affecting a broad range of properties. A simple, mildly-conditioned (low pressure at 7 MPa, for 0–25 cycles) homogenization approach was explored, and its effects on the Northern bleached softwood based-CNF films' functional properties were investigated. Post-homogenization, promoted hydrogen bonding and fibrillation were evidenced by FTIR and surface SEM, respectively. A maintained high crystallinity (64 %) and smoother surface of homogenized CNF films (Sa, 2.64 from 4.73 μm) compared to the untreated CNF films was also achieved. The resulting decrease in oxygen permeability (0.25 from 0.48 cc.μm/m^2.day.kPa, at 50 %RH) is comparable to the reference values of the commercial oxygen barrier resin brand of ethylene-vinyl alcohol (EVOH). Significant improvements in mechanical (tensile strength, 157 from 94 MPa; Young's modulus, 3843 from 2630 MPa; and elongation-at-break, 7.59 from 5.69 %) and thermal (elastic modulus, loss modulus, damping factor, and degradation temperature) properties were confirmed. Contact angle improvement (0–60 s) was also obtained. With varying optimum homogenization cycles, this work demonstrates the prospect of a straightforward, cheap, and environmentally friendly approach in modifying CNF with enhanced processability and applicability for diverse applications.

1. Introduction

Americans waste 40 % of their food, costing 1.3 % of GDP (EPA, 2016; FAO, 2013; FAO, 2021). Food spoilage is mainly triggered by microbes, H_2O, O_2, temperature, and light (Magoulas, 2016). Food and its packaging comprise roughly 45 % of the solid wastes landfilled in the USA (EPA, 2015). Globally, one-third of agricultural land is used to grow food that ends up wasted every year, releasing greenhouse gases (UNEP, 2024). Around 98 % of single-use plastics (e.g., polyethylene, polypropylene, polyethylene terephthalate), including those used in food packaging applications, are made of non-sustainable or non-biodegradable fossil fuel (Charles & Kimman, 2023; Tun et al., 2023) and roughly 80 % became wastes (Geyer et al., 2017). Composting merely covers 6 % due to limitations in infrastructure, expensive labor, materials, and contamination (NRDC, 2020; ReFED, 2018). Meanwhile, only 12 % and 9 % are incinerated and recycled, respectively, with challenges including losses, degradation, mechanical performance, cost, complexity, and release of CO_2, toxic chemicals, micro-/nano-plastics, or volatile organic compounds, with the rest ultimately contaminating soil and water (Birkett et al., 2017; Byun et al., 2015; Geyer et al., 2017; UNEP, 2022). However, due to the urbanization-led global dietary change and reliance on processed foods (World Packaging Organisation, 2008), food packaging remains in high demand.

In response to these lingering issues on food (packaging) wastes, "prevention" (e.g., spoilage-prevention primary packaging) is encouraged over "recovery" and "recycling" (EPA, 2016; European Commission, 2023; FAO, 2022). Thus, studies on shelf-life extension through barrier features to suppress spoilage rates are continually advancing (Almenar, 2023; Verghese et al., 2015). Likewise, research on packaging materials with biodegradability in various environmental conditions has also been prioritized. The Earth's most abundant naturally biodegradable polymer is cellulose (Klemm et al., 1998). Cellulose comprises several linear β-(1,4)-D-glucose chains joined by inter-/intra-molecular hydrogen bonding and van der Waals forces, forming (micro)fibril structures (Liu et al., 2023). Cellulose can be converted into two 'top--down' nanosized products to create a more extensive network structure (Lee et al., 2017). The first is the rigid rod-like cellulose nanocrystals (CNC), prepared chemically (e.g., acid hydrolysis, oxidation,

* Corresponding author.
E-mail address: ytkim@vt.edu (Y.-T. Kim).

https://doi.org/10.1016/j.carpta.2025.100739

Available online 4 March 2025

cationization) to remove amorphous region, leaving purely-crystallines. Meanwhile, the second is the flexible cellulose nanofibrils (CNF), prepared mechanically (e.g., micro-fluidization, homogenization, grinding, sonication), to preserve both amorphous and crystalline regions (Dias et al., 2020; Ibrahim et al., 2019; Sofla et al., 2016).

Sometimes referred to as cellulose nanofibers or nanofibrillated cellulose, CNF is among the most researched due to its high specific surface area, crystallinity, surface activity, barrier ability, and an even better aspect ratio than CNC, while having low porosity and density (Yang et al., 2019). In the past decades, many have researched the growing potential of CNF in improving barrier properties (Aulin et al., 2010; Fukuzumi et al., 2013; Fukuzumi et al., 2009; Roilo et al., 2018) and biodegradability in diverse environments (Arun et al., 2022; Babaee et al., 2015; Niu et al., 2021; S. Xu et al., 2021). Softwood-based CNF, precisely one derived from northern bleached softwood kraft pulp, was selected for this work. Besides being the first raw material (Herrick et al., 1983; Turbak et al., 1983) and today's most popular (Lee et al., 2017), softwood-based CNF was more flexible and responsive to be fibrillated than hardwood, whose spirally-layered outer secondary wall reduces flexibility and accessibility to the inner secondary wall (Stelte & Sanadi, 2009). Softwood is also easier to modify chemically due to glucomannan being the dominant component of its hemicellulose, which contains C6 primary hydroxyls and is easily convertible into other functional groups. In contrast, hardwood's hemicellulose is mainly xylan that lacks C6 primary hydroxyl groups. Films produced using softwood-CNF also possessed a higher light transmittance (Fukuzumi et al., 2009; Sjostrom, 2013).

However, CNF still possesses some constraints that hinder processability and applicability compared to conventional polymers. Although hydrophilic/hygroscopic by nature, cellulose in its native form is insoluble and non-redispersible in water and most organic solvents due to crystallinity and extensive strong intra-/inter-molecular hydrogen bonds between individual chains (Etale et al., 2023; Lavoine et al., 2012; Nechyporchuk et al., 2016; Zuppolini et al., 2022). Moisture absorption could also cause swelling that disrupts strength, durability, barrier ability, and thermal stability (Xia et al., 2018; Yang et al., 2019). As the solution to the aforesaid challenges, homogenization is among the most popular treatments for cellulose-based materials as it does not require high temperatures and organic solvents or chemicals other than simply water, highlighting its simplicity and environmental friendliness (Wang et al., 2021). Cellulose-based aqueous suspension is pumped through a spring-loaded valve assembly that opens and closes repetitively, allowing the suspension to be subjected to certain pressure drops, inducing high shear, cavitation, and impact forces in the narrow slit of the valve. It promotes fibrillation and the subsequent hydrogen bonding and 3D network strength (Chun et al., 2011; Lee et al., 2017; Nagarajan et al., 2021). Structural stability would be improved since homogenization affects rheology, particle size, surface area contact, and distribution/-dispersity before and after the film drying stage, especially for polysaccharides like CNF (Cheng et al., 2010; Flores et al., 2021; Usenko et al., 2013).

Homogenization is categorized based on the conditioning pressure range, namely ultra-high (>250 MPa), high (50–250 MPa), and low (<50 MPa) (Aguayo et al., 2017). However, the most notorious drawback of conventional homogenization is the high pressure that leads to, not only high energy consumption and cost (Boulemkahel et al., 2021; Lee et al., 2017; Nagarajan et al., 2021), but also crystallinity loss due to surface crystallites peeling off under high shear and impact forces (Davoudpour et al., 2015). Therefore, lower pressure homogenization is prospective for treating CNF, which has yet to be studied. Multiple passes or cycles are often required in homogenization (Nakagaito & Yano, 2004), where the number of cycles determines the final homogenates' degree of fibrillation and subsequent properties (Davoudpour et al., 2015; Kalia et al., 2014). Some even emphasized the importance of the number of passes over other homogenization operating conditions, including pressure (Fu et al., 2011; Yu et al., 2021). Another common challenge in homogenization is clogging (Lee et al., 2017; Nagarajan et al., 2021). Thus, a homogenizer equipped with the novel, patented modular 'emulsifying cells' was explored in this work. The parallel flow setup has several alternating orifices that allow material to flow in one direction and exit from the opposite end of the nozzle. Due to its absorption-inducing reactors, this design replicates multiple homogenization passes with the cost/time efficiency of merely 1–2 passes. The emulsifying cell also excels with its tailorable shear/cavitation/impact forces, pressure, flow, and duration, as well as the minimal heat buildup after the advanced cooling systems (Pion, 2015; Pion, 2024). This essentially prevents clogging, agglomeration/aggregation, and destruction in the resultant CNF films due to over-shearing/pressure/heating. Such an approach has been evidenced to be fruitful in an array of materials, including CNF-based products where the effect of varying cycles and pressures were investigated, e.g., 8 cycles/151 MPa (Li et al., 2018), 5 cycles/69–207 MPa (Cheng & Via, 2017), 10–30 cycles/70–310 MPa (Lee et al., 2018), 3 cycles/160 MPa (Du et al., 2016), and 4–20 cycles/110–290 MPa (Wang & Drzal, 2012). However, utilizing the aforesaid 'emulsifying cell' based homogenization at low pressure, especially on CNF modification, has yet to be explored.

Ultimately, the development of softwood-based CNF film treated with a milder-conditioned homogenization in varying cycles was conducted. The goal of this work was to determine the effectiveness of such a novelty in the homogenization approach (low-pressured and 'emulsifying cells'-equipped) in modifying CNF. The effect of the number of homogenization cycles was hypothesized to promote the fibrillation of CNF that governs the final product's functional properties, including, but not limited to, physical, mechanical, morphological, and thermal stability.

2. Materials and methods

2.1. Materials

CNF slurry (3 % solids) of northern bleached softwood kraft pulp was from the Process Development Center of the University of Maine (Orono, ME, USA). According to the product's safety data sheet, technical and specification reports (Amini et al., 2020; Sluiter et al., 2008; Y. University of Maine, 2017; Y. University of Maine, 2017), its weight percentages of constituents were 78 % cellulose, 20 % hemicellulose, and 2 % lignin; with nominal fiber width of 50 nm and lengths of up to several hundred microns; and surface charge (zeta potential) of −48 to −5 mV. HPLC-grade water was purchased from EMD Millipore (Burlington, MA, USA).

2.2. Homogenization process

CNF slurry (3 % solids) was diluted with water (1:3, 30 mins) to obtain neat-CNF solution. The solution was further treated with a Mini DeBEE 30 homogenizer (Pion Inc., Billerica, MA, USA) with a 0.2 mm (0.008 inch) nozzle at 7 MPa, repeated for a different number of cycles (0, 5, 10, 15, 20, 25; N-0, N-5, N-10, N-15, N-20, N-25, respectively). The cycles were maintained <30 referring to optimized results of previous studies on homogenized cellulose modified at a medium and low conditioning pressure range (Cheng & Via, 2017; Chun et al., 2011; Du et al., 2016; Lee et al., 2018; Li et al., 2018; Wang & Drzal, 2012). The internal cooling system was followed by the use of an isotemp refrigerated circulating bath 910 chiller (Fisher Scientific, Waltham, MA, USA).

2.3. Film production

The homogenized CNF solution (30 mL) was solvent-casted into a petri dish (9 × 1.5 cm) and left to dry in the Forma environmental chamber (Thermo Scientific, Waltham, MA, USA) (50 %RH, 23 °C, 48 h). The same preconditioning was conducted prior to each test of the films,

as listed below. One-way variance analysis (ANOVA) followed by Tukey's was conducted, where different letters denote statistically significant differences (p-value ≤ 0.05).

2.4. Fourier transform infrared (FTIR) analysis

Nicolet 8700 FTIR–Attenuated Total Reflectance (ATR) spectroscopy (Thermo Scientific, Waltham, MA, USA) was used to produce spectra that plot 32 scans of wavenumber (400–4000 cm^{-1}) vs IR absorbance.

2.5. Crystallinity

The employed D8 x-ray diffraction (XRD) (40 kV; 40 mA; Cu Kα irradiation: λ, 1.54056 and Å, 0.154 nm; 1181 steps; $2\theta = 5–35°$; 0.025° increment; 0.5 s) (Bruker Corporation, Billerica, MA, USA) was equipped with "twin/twin" optics ("Motorized Slit: Slit-width"; primary, 0.6 mm; secondary, 5 mm) and cooler (15–20 °C). The resulting data in *.brml* format were processed using PowDLL (Kourkoumelis, 2013) or Profex (Doebelin & Kleeberg, 2015) software to produce spectra that plot XRD angle (2θ) vs intensity.

$$CI = \left(1 - \frac{I_{am}}{I_{total}}\right) \times 100\% \quad (1)$$

The popular, easy, and time-efficient Segal's "height" method was used to determine the crystallinity index (CI), or mass ratio of crystalline substance in the total dry sample based on crystallographic two-phase model. The intensity ratio formula between spectra's crystalline and amorphous peaks is above (Eq. (1)), where I_{am} is the minimum intensity of amorphous peak (or the maximum point where the entirely amorphous region is located) at $2\theta = \sim18–19°$, and I_{total} is the maximum intensity of crystalline/major peak at $2\theta = \sim22–23°$ (Daicho et al., 2018; Nurhadi et al., 2022; Park et al., 2010; Segal et al., 1959).

2.6. Morphology and roughness

Sample (25 mL) was kept in a Forma 88,000 ultra-low freezer (−80 °C, 1 h) (Thermo Scientific, Waltham, MA, USA) prior being sent to a benchtop freeze-dryer (−40 °C, 1 h) (Millrock Technology, Kingston, NY, USA). Dry sample was then mounted onto a pin stub using copper tape before being coated with gold (100 Å) using argon gas (10–15 psi) in an ion sputter coater (50 mTorr, 45 milliamps, 45 s) (Denton Vacuum, Moorestown, NJ USA). Morphology was imaged at different magnifications using NeoScope JCM 5000 Scanning Electron Microscope (SEM) (10 kV) (JEOL Ltd., Tokyo, Japan).

In regard to roughness, surface irregularities height is expressed by the arithmetic mean deviation of the height of a line, or *Ra*. The extension of *Ra* to a surface, *Sa*, is the difference in height compared to the surface's arithmetical mean. Simply put, Ra is the average of the surface heights along a measurement trace, while *Sa* is the average roughness over a measurement area (Adamčík et al., 2023; Keyence, 2021; Mike, 2022; Woch et al., 2022). Keyence VK-X3000 3D (Keyence Corporation, Osaka, Japan) was used referring to ISO 25,178, where the produced 3D and z-stack images of the specimen surface were analyzed with the MultiFileAnalyzer software to perform filtering according to reference plane to the real surface to smooth out height variability.

2.7. Transparency

In addition to naked-eye detection, Genesys 10S ultraviolet-visible (UV–vis) spectrophotometer (Thermo Scientific, Waltham, MA, USA) was used to produce spectra that plot wavelength (190–900 nm, 0.5 nm interval) vs light transmittance.

2.8. Barrier property

The 700–118–20 Quick Mini digital thickness gauge (Mitutoyo, Kawasaki, Japan) was used for ten readings to the nearest 0.001 mm. The C230 Oxygen Transmission Rate (OTR) Testing System (Labthink International Inc., Medford, MA, USA) was employed according to ASTM D 3985–95 with the "Film-ASTM" test type without compensation selected (preheating 2 h, 100 mL/min, 50 %RH, 23 °C, referring to ASTM). To maintain purity, cycle process mode with rezero purging for nitrogen gas in the cells was performed (30 s, one cycle interval). Cycles under standard test mode were completed at 30-min intervals in each cell to obtain oxygen (O_2) permeability (OP) values.

2.9. Mechanical properties

The Universal Testing Machine MTS 10-GL 27–00,112 (MTS Systems Corporation, Eden Prairie, MN, USA) was used according to ASTM D638–22 (ASTM, 2022). The stress-strain relationship was determined by applying tension/compression in a steadily increasing axial force to the sample to determine the following mechanical behaviors: 1) tensile/ultimate strength (TS); 2) elastic/Young's/tensile modulus or relative stiffness or rigidity (E); and 3) elongation-at-break or fracture strain or ductility (EAB). TS, E, and EAB of the films (2 × 8 cm; 50 %RH, 23 °C) were measured with 0.1 N preload at a test speed of 0.40 mm/s.

2.10. Thermal properties

The Discovery Q850 Dynamic Mechanical Analyzer (DMA) (TA Instruments, New Castle, DE, USA) was employed by loading sample strips (13 × 7 mm) using dual screw film clamp type. The 0.05 %-oscillatory multi-frequency strain, static force of 0.01 N in tension, and temperature ramp (−60–150 °C; 5 °C/min) were applied. Force track and soak times were adjusted to 125 % and 5 min, respectively. Viscoelastic behaviors (elastic/storage modulus (E'), loss/imaginary modulus (E"), loss/damping factor/tangent ($\tan\delta = E"/E'$)) were recorded at 1 Hz.

Next, Thermogravimetric Analyzer (TGA) 550 (TA Instruments, New Castle, DE, USA) was conducted. Pan loading-taring was performed using the auto sampling technique, where sample (5–15 mg) was spread in the 100 μL-platinum pan to maximize surface area. Temperature was equilibrated at 50 °C, then ramped to 700 °C (10 °C/minute). Temperature when the sample reached 5 %-degradation ($T_{d,5\ \%}$) was recorded. Data was analyzed using the TRIOS/TA Universal Analysis (TA Instruments, New Castle, DE, USA) software.

2.11. Contact angle

The OneAttension® Theta Flow optical tensiometer (Biolin Scientific, Stockholm, Sweden) was employed. Using the "sessile drop" experiment type with a 200 μL pipette tip at 25 μL/min dispenser speed, a water drop (5 μL) was deposited onto the film surface. "Light" and "heavy" phases were set as air and water (20 °C), respectively, to determine density difference for surface tension measurement. The drop images and contact angles were obtained with a total duration of 60 s at ten-second intervals.

3. Results and discussion

3.1. Fourier transform infrared (FTIR) analysis

Fig. 1 illustrates the chemical structure of cellulose, whose major functional groups' presence was discussed through FTIR spectra findings. Table 1 lists the approximate wavenumber (cm^{-1}) of dominant peaks/bands and their assigned functional groups/bonds and molecular vibration type (Morán et al., 2008; Soni et al., 2015). The intra/inter-molecular hydrogen bond was characterized by the observed O–H stretching vibrations belonging to hydroxyl groups (–OH) in all

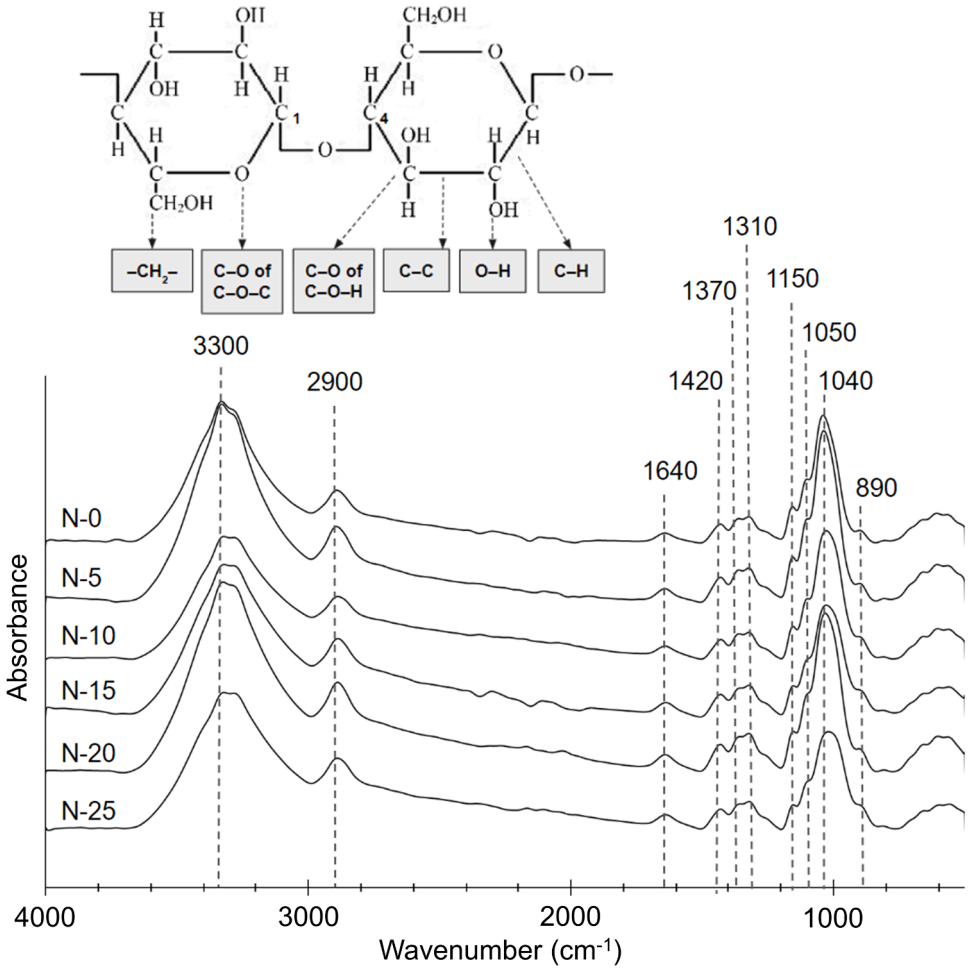

Fig. 1. Chemical structure of cellulose and FTIR spectra of freeze-dried CNFs.

Table 1
FTIR peaks assignment of freeze-dried CNFs.

Wavenumber (cm^{-1})	Molecular vibration type and functional group/bond
3300–3340	Stretching; O–H
2900	(A)symmetrical stretching; C–H of CH_2 (methylene)
1640	Bending; O–H of H_2O (water)
1420	Scissoring; C–H of CH_2 (methylene); cellulose's crystalline
1370	Bending; C–H and C–O
1310	Wagging; C–H of CH_2 (methylene)
1150	Stretching; C–C
1040–1050	Asymmetrical stretching; C–O of C–O–C of pyranose ring
890	Cellulose's amorphous; β–1,4–glycosidic linkages

CNFs. Likewise, C–H, C–C, and C–O occurred not only as glycosidic linkages but also within pyranose rings of glucose units. The O–H bands of H_2O were also present in all spectra, indicating the remaining moisture even post-drying due to cellulose-H_2O interaction (Korhonen et al., 2011; Morán et al., 2008). Nevertheless, freeze-dried CNFs were used instead of films to produce spectra with more obvious peaks/bands. Other volatile degradation products that would be emitted during freeze-drying could also be hydrocarbons (3100–2600 cm^{-1}), CO_2 (2420–2240 cm^{-1}), CO (2240–2040 cm^{-1}), C = O (1800–1600 cm^{-1}), and C–O (1130–1050 cm^{-1}) (Quiévy et al., 2010)—all unapparent in freeze-dried CNFs' spectra. Conclusively, no new bonds were formed post-homogenization, indicating no chemical composition change, as seen in similar studies (Huang et al., 2020; Ilyas et al., 2019). The peaks at 890 and 1420 cm^{-1} (Akerholm et al., 2004; Schultz et al., 1985) also confirmed that the desired high crystallinity of CNF was successfully maintained despite the mechanical treatment, whose in-depth analysis by XRD is discussed in the next section. All spectra discussed were similarly observed in other studies on homogenization impact on cellulose-based materials (Huang et al., 2020; Quiévy et al., 2010; Shamskar et al., 2019).

3.2. Crystallinity

Fig. 2 presents the diffraction peaks of CNF film. Based on previous reports (Hafez et al., 2020; Manimaran et al., 2019; Siti Syazwani et al., 2022; SriBala et al., 2016; Zhao et al., 2019), the resulting patterns were categorized into Cellulose I type whose characteristic peaks were the Miller indices of $(1\bar{1}0)$ at $2\theta = 15°$, (110) at $2\theta = 17°$, (200) at $2\theta = 22.5°$, and (004) at $2\theta = 35°$ (Liu et al., 2022). Despite the mechanical treatment, CNFs retained the crystallinity and structure of the native cellulose in the rawest form of softwood as found in nature. Minuscule peaks arising at $2\theta = 25°$, 28.5° and 32° were attributed to the crystalline phase of impurities/trace elements or residual salts. No significant difference in crystallinity index (CI) (averaging 64 %) signified the applied low-pressure, multicycle homogenization (7 MPa for 0–25 cycles) did not significantly alter the molecular structure and crystalline rearrangement, as reported previously, e.g., 30–50 MPa for 0–3 cycles (Boulemkahel et al., 2021), 30–60 MPa for one cycle (Kasemwong et al., 2011), and 60 MPa for one cycle (Wang et al., 2008). These were in contrast to the considerable effects on crystallinity of CNFs homogenized under higher pressure and cycles, e.g., 20–50 MPa for 20–40 cycles (Davoudpour et al., 2015), 40 MPa for 4 cycles (Liu et al., 2023), 140 MPa for 4–20 cycles (Chun et al., 2011), and 150 MPa for 0–20

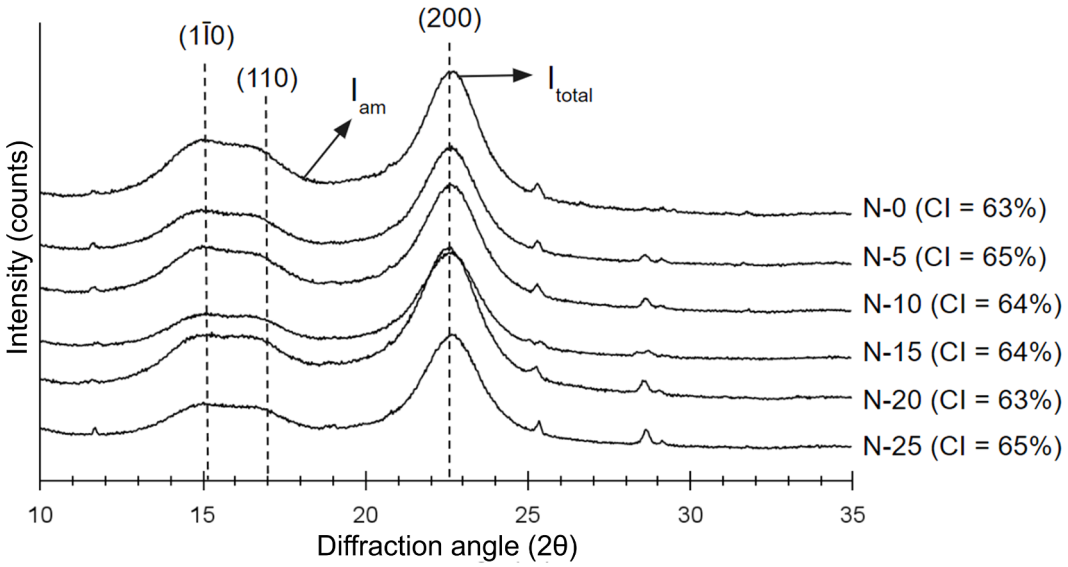

Fig. 2. XRD spectra and CI of CNF films.

cycles (Ueda et al., 2022). Though mechanical treatment promotes water binding capacity and gel-like structure formation (Ulbrich & Flöter, 2014), harsh conditions including excessive homogenization pressure and number of passes might lead to the destruction of (sub) crystal zones and covalent bonds (Hoover & Ratnayake, 2002). Particles passing through the "high-energy zone" resulted in aggravated particle structure and compact layer structure damage, decreased amorphous region stability, and branched the crystal region's molecules to be cut into short straight-chain ones (Guo et al., 2019; Meng et al., 2014). Despite this work's multiple homogenization passes, this finding highlighted the success perseverance of CNF's crystallinity due to the low pressure, especially suitable to certain processing where the preserved long cellulose chain is essential, e.g., reinforcement agent (Yano et al., 2018) and thermal-conductive filler (Lou et al., 2021).

3.3. Morphology and roughness

The surface morphological images of freeze-dried CNFs are presented in Fig. 3(a). Freeze-dried specimen was preferred during microscopic visualization due to dehydration and subsequently preserved nanoparticles integrity and porosity (Abdelwahed et al., 2006; Lee & Chow, 2012; Palmkron et al., 2023; Vasconcellos & Farinas, 2018); thus, the CNFs fibrillation post-homogenization could be highlighted. Prior homogenization (N-0) images showed rough and unevenly-thick bundles (average width, 8–10 μm) of compactly entangled fibrils. Post-homogenization even after minimum cycles (N-5), the degree of fibrillation was improved due to the provided shear impact as the suspensions flew through tiny gaps under intensive shear (Wang et al., 2021). Fibrils began to loosen and detach from each other, significantly reducing the bundles' dimensions, even releasing individual fibrils with nanosized diameter. The increased specific surface areas eventually promoted hydrogen bonding with water (Kose et al., 2011). With the more homogenization cycles, the more extensive and complex web of thin, fine, and long fibrils was formed, especially in N-15. However, the over-shearing was apparent in the higher number of homogenization passes (N-20/25), indicated by the aggregation and agglomeration of individual fibrils possibly caused by excessive mechanical treatment as observed in previous works including ones with higher pressure homogenization approach (Dilamian & Noroozi, 2019; Kose et al., 2011; Malucelli et al., 2018; Pelissari et al., 2017).

The roughness of CNF films was presented in *Sa* values (Fig. 3(b) and **Table S1**) and microscopic images (**Fig. S1**). Top surface was specifically selected due to the film solvent casting method that led to the smoother bottom surface as it was dried out directly on the petri dish and such a varying microstructure might affect wettability, porosity, and pore size (Jagodzińska et al., 2021; McGaughey et al., 2020). Minimum cycles of homogenization (N-5) managed to significantly decrease the CNF film's roughness (44 % smoother). However, the effect of over-shearing became apparent after 20 passes (N-20), where the film surface started to regain roughness although still 27 %-smoother than the control. This phenomenon was aligned with morphology findings (Fig. 3(a)) and perhaps after the protuberance prominences on the surface, regardless of the occurrence of aggregation (Xue et al., 2021; Żołek-Tryznowska et al., 2023). Micro-pores likely existed in locations along the thicker parts of the N-20, usually attributed to more residual fibers—the non-fibrillated microscopic fibers and fiber fragments that might contribute to a rougher surface (Chinga-Carrasco et al., 2014; Miettinen et al., 2014; Nechyporchuk et al., 2016). Overall, the obtained range of *Sa* values was comparable to that of high-pressured, homogenized CNF reports (Miettinen et al., 2014). Other roughness profiles investigated were 3D and z-stack microscopic images (**Fig. S1**) confirming the findings even further on the homogenized films' smoother surfaces. Smooth CNF films are potential in gloss finishes applications; meanwhile, the roughly-surfaced ones possess noteworthy implications on electrical behavior when used in field-effect transistors (Lehmann & Zahn, 2009). The prospect of smooth cellulose-based films as food packaging has been explored (Chen et al., 2014; Han et al., 2024; Huang & Wang, 2022).

3.4. Transparency

Fig. 4 displays the UV–vis spectra paired with naked-eye detection of CNF films. Homogenized films were significantly more transparent (higher %-light transmittance) due to the enhanced fibrillation (Dinesh & Kandasubramanian, 2022). N-20 displayed the best transparency among all films (56 %-transmittance at 900 nm), nearly thrice as transparent as the control (20 %-transmittance at 900 nm) and superior to other nanocellulose reports (Herrera, 2015; Herrera et al., 2012; Sun et al., 2018). However, decreasing transparency was observed eventually due to over-shearing. Though fibril aggregation and agglomeration started at N-20 as discussed in surface morphological (Fig. 3(a)) and roughness' 3D/z-stack (Fig. 3(b), **S1**) findings, it only became impactful enough to the ability of light to pass through at N-25 which led to more scattered light and decreased optical transmittance (Lizundia et al., 2016), as formerly reported (Cheng et al., 2015).

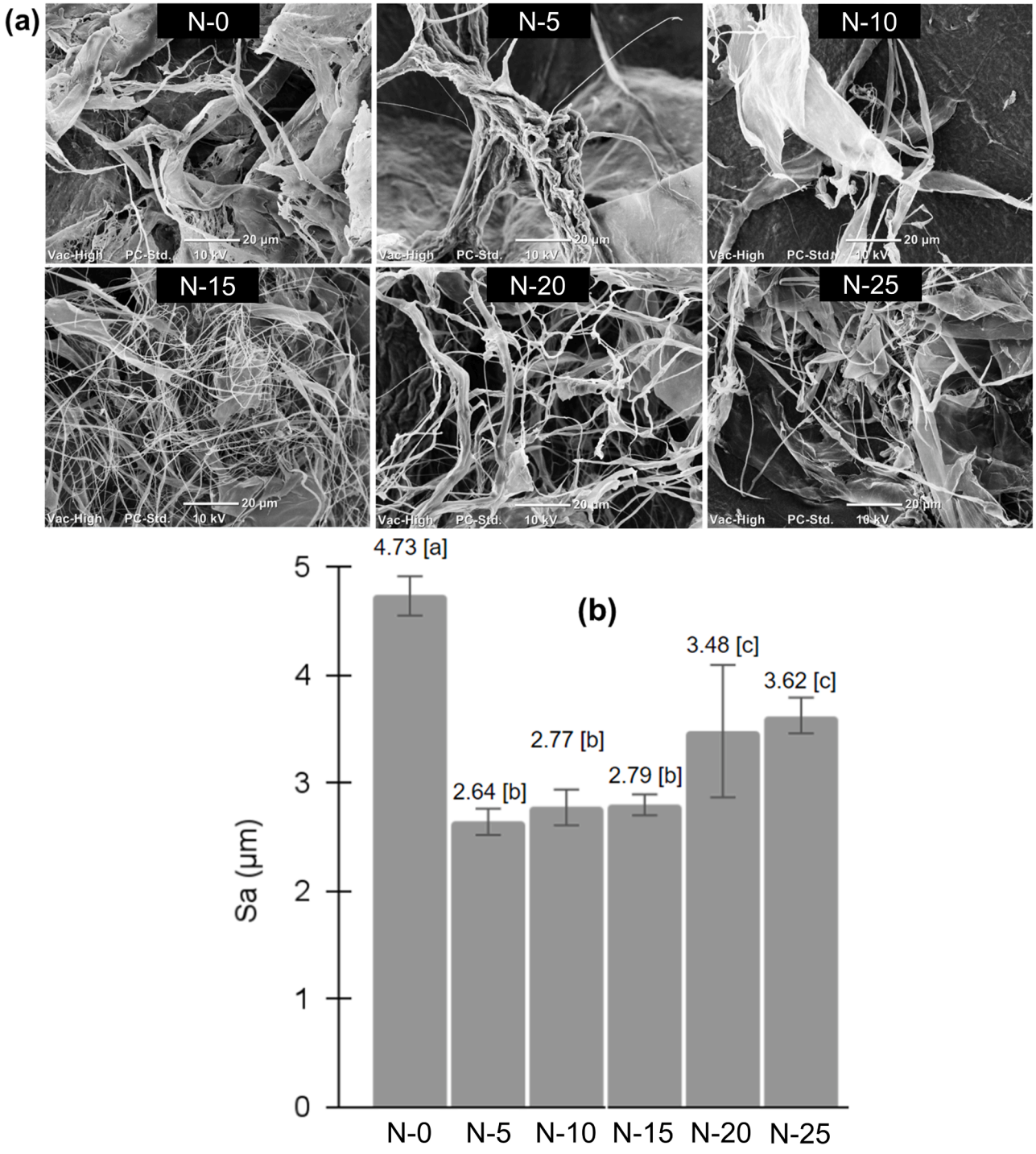

Fig. 3. (**a**) Surface SEM images (1000 x); and (**b**) roughness (*Sa*) of CNFs.

3.5. Barrier property

Fig. 5(a) and **Table S1** present the thickness of CNF films. The films became thinner the higher the homogenization cycles, whose values are comparable to former studies (Dogan & McHugh, 2007; Kittle et al., 2018; J. Wang et al., 2018; Y. Xu et al., 2021). Furthermore, Fig. 5(b) and **Table S1** display the O_2 permeability (OP) of CNF films at 50 %RH, where the O_2 diffusion path is illustrated in Fig. 5(b). OP significantly decreased by 48 % after minimum cycles of homogenization (N-5), implying the impact of promoted fibrillation post-homogenization that enhanced hydrogen bonding, creating a more densely packed structure (Peresin et al., 2017), as also evidenced in morphological findings (Fig. 3 (a)). OP increased when more passes of homogenization were applied presumably after fibril length reduction as the over-shearing aftermath, as reported where the initially observed long fibrils at small numbers disappeared with continued mechanical treatment, alongside the appearance of newly-produced fibrils (Redlinger-Pohn et al., 2022; Zhou et al., 2018). Instead of the long fibrils with a high aspect ratio turning and entangling into a web structure, the hydrogen-bonded shorter fibrils and subsequent more void volumes made a significantly less tortuous diffusion path for O_2 (Wang et al., 2020). Therefore, despite the promoted fibrillation, N-10 and beyond suffered from worsened barrier ability. Film thinness could be another reason for the rising OP (Aulin et al., 2010; Kittle et al., 2018; J. Wang et al., 2018).

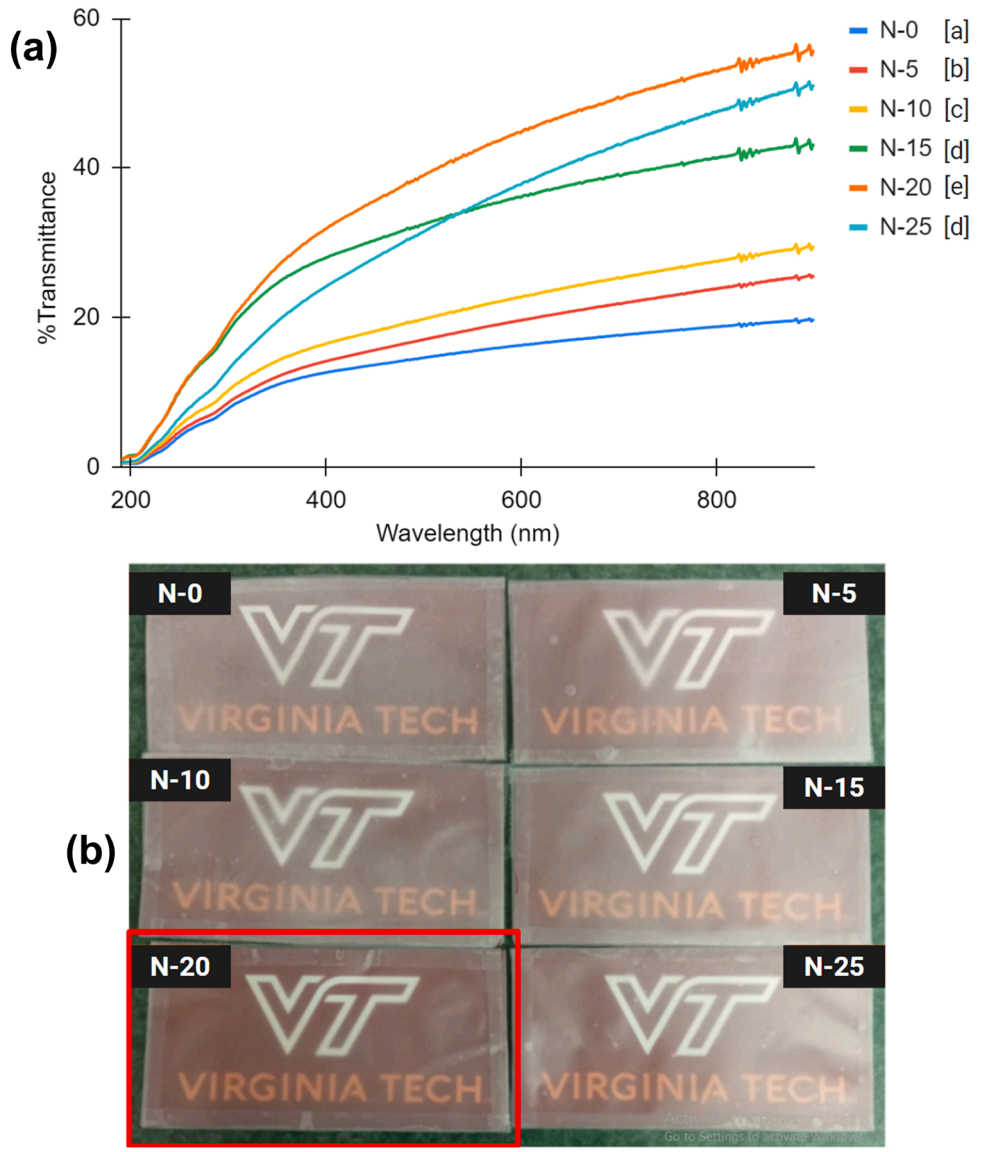

Fig. 4. Transparency of CNF films: (**a**) UV–vis spectra; (**b**) naked-eye detection.

The best obtained value (N-5) was compared with ethylene vinyl alcohol (EVOH), a commercial polymer with exceptional O_2 permeability usually applied in multilayer structures with other polymers. EVOH composition dictates its performance and 25–45 mol % ethylene content is required for high barrier resin standards (Artzi et al., 2005). N-5 possessed a noteworthy barrier performance (0.250 cc.μm/m^2.day.kPa) compared to EVOH products, falling between EVOH38 and EVOH44 (38 and 44 mol % ethylene, respectively), in particular H and E type of the EVAL™ brand (0.099–0.138 and 0.197–0.375 cc.μm/m^2.day.kPa, respectively) (Kuraray, 1972). OP of N-5 was also notably superior against several common synthetic, O_2 barrier plastics, i.e., PVA, MXD6, PET, and PVC at 0.197–9.869, 0.493, 10–50, and 20–79 cc.μm/m^2.day.kPa, respectively, even some PVDC (0.099–2.961 cc.μm/m^2.day.kPa), at 50 %RH (Michiels et al., 2017). This work's finding also exceled over other CNF-based high barrier films, e.g., CNF composite, filtered-pressed CNF, carboxymethylated CNF, and carboxylated CNFs, at 0.470, 0.600, 0.365, and 0.622 cc.μm/m^2.day.kPa (Aulin et al., 2010; Kumar et al., 2014; Liu et al., 2011; Nair et al., 2014; Osterberg et al., 2013; Siró et al., 2011; J. Wang et al., 2018). Remarkable barrier property is among cellulose's numerous advantages. In regard to its applicability as food/pharmaceutical packaging, OP is responsible for many degradation processes, e.g., lipid oxidation, microorganism growth, enzymatic browning, and losses in flavor, color, and nutrients; even identified as the most common cause of packaged product's quality loss (Ayranci & Tunc, 2003; Brown, 1992; Hong & Krochta, 2006). Despite the necessary presence of O_2 for any living tissue's respiration, O_2 also accelerates ethylene production, leading to senescence (Oms-Oliu et al., 2008; Rojas-Graü et al., 2007). OP provides protection necessary to achieve the desired shelf life of a product whose O_2 sensitivity may vary (Koontz, 2016). Due to humidity, CNF's hydrophilicity led to swelling and moisture-absorbing tendencies of hydroxyl groups, allowing the water to replace hydrogen bonds, loosening the structure, and eventually allowing gases, such as O_2, to penetrate and diffuse.

3.6. *Mechanical properties*

Fig. 6 and **Table S1** display the mechanical properties of CNF films. Tensile strength (TS) determines the maximum stresses one can withstand before falling, while elastic modulus (E) defines how much one would deflect (structural displacement) under an applied load, and elongation-at-break (EAB) implies one's resistance to shape changes without cracking (Djafari Petroudy, 2017; Jain et al., 2009; Jurowski & Grzeszczyk, 2015; Koo et al., 2017; Pavlík et al., 2019). The highest TS, E, EAB were achieved by N-10, N-15, N-5, roughly 67 %, 46 %, 33 %

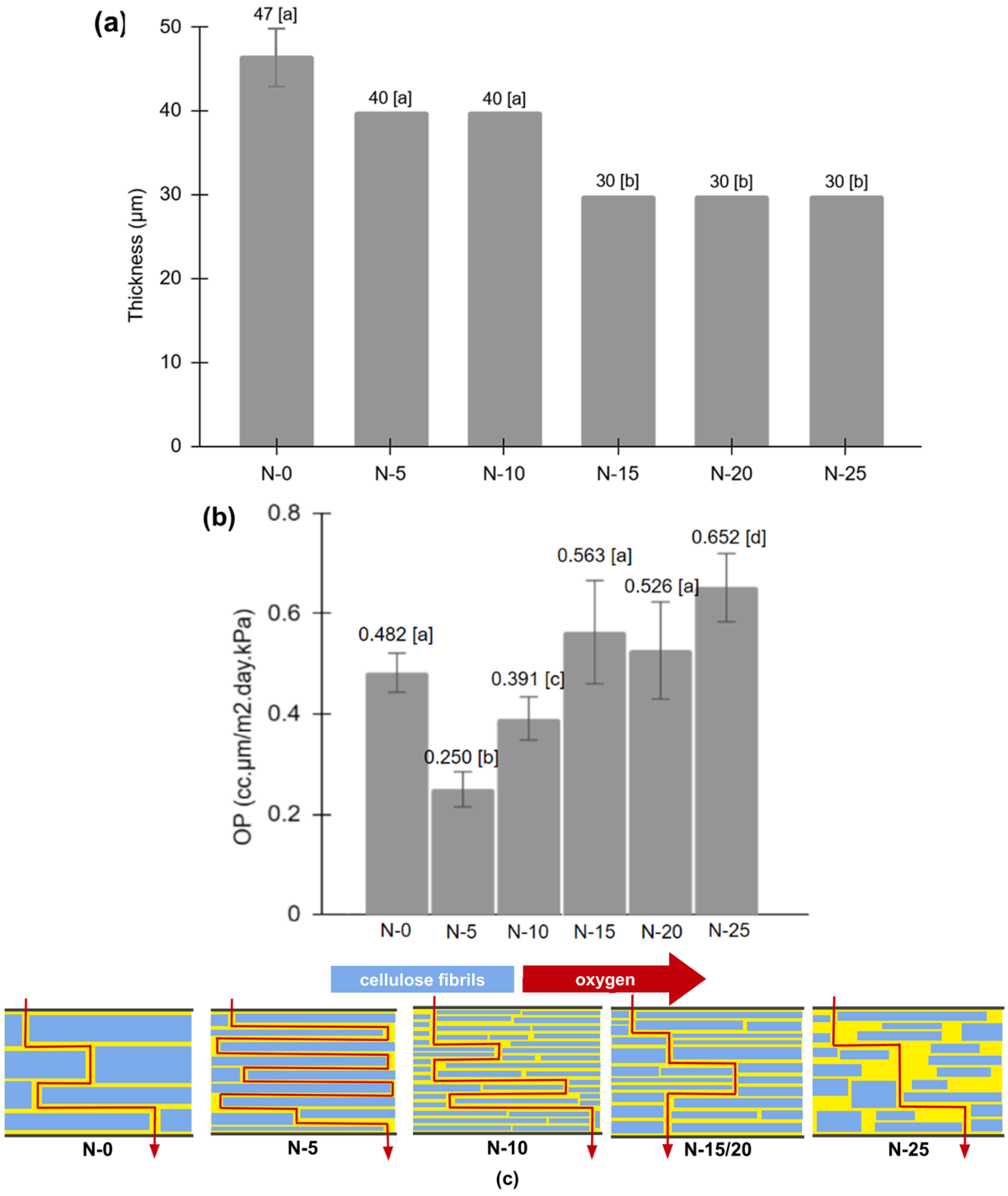

Fig. 5. (**a**) Thickness and (**b**) OP of CNF films at 50 %RH; and (**b**) illustration of oxygen diffusion paths comparison.

increase from the control's, respectively. These proved the promoted fibrillation association with the increased resistance from rupturing. The observed 'plateauing' was similarly found in other homogenized cellulose reports (Iwamoto et al., 2007; Josset et al., 2014; Naderi et al., 2015; Spence et al., 2010). However, EAB is highly influenced by aspect ratio, thus, CNFs with a lower aspect ratio post-homogenization (N-10 and beyond) were rigid and easy to pull out from the aggregated/agglomerated fibers (Pelissari et al., 2017; Saïd Azizi Samir et al., 2004), similarly discussed in surface roughness (Fig. 3(b)) and OP findings (Fig. 5). Overall, N-25 showcased the most obvious effect of 'over--shearing' as highlighted in other properties. Aggregation/agglomeration impaired contact among fibrils and weakened the structure, making it more prone to rupture, as evident in other CNF studies (Malucelli et al., 2018; Pelissari et al., 2017). Fibril-fibril hydrogen bonding facilitates stress transfer and is influenced by dimensions, orientation, surface functionalities, counterions, and porosity. Strong interfacial adhesion eases stress distribution during deformation, improving strength due to the repeated breakage/reformation of hydrogen bonds between neighboring fibrils and energy dissipation under stress (Mokhena et al., 2021). Overall, these mechanical trait findings are comparable to others (Atiqah et al., 2019; Fein et al., 2021; Malucelli et al., 2018; Pelissari et al., 2017).

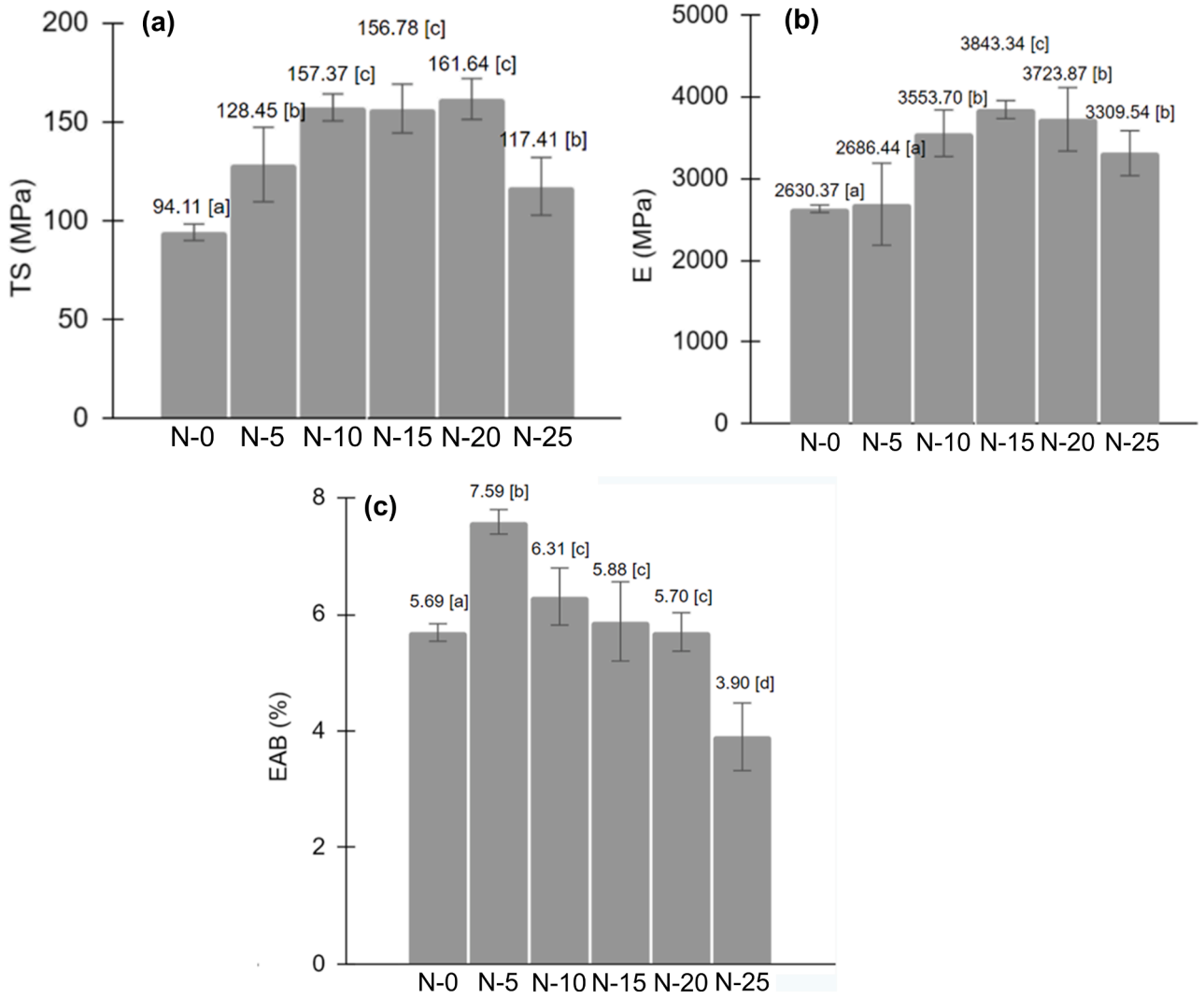

Fig. 6. Mechanical properties of CNF films: (**a**) TS, (**b**) E, and (**c**) EAB.

3.7. Thermal properties

Thermo-dynamic mechanical analysis (DMA) results of elastic/storage modulus (E'), loss/imaginary modulus (E"), loss/damping factor/tangent (Tanδ) and each highlighted values at 25 and 100 °C as the reference temperatures (Kwan, 1998) are presented in Fig. 7**, Fig. S2,** and **Table S2**. E' (Fig. 7(a)) defines strength, stiffness, and rigidity; decreases as temperature increases, and increases again to a maximum value because of structural change, before decreasing back after glass transition temperature and reaching the final cure due to thermal degradation and devitrification (Candan et al., 2016; Sanyang et al., 2016). At low temperatures, E' remained constant (~2–3 GPa) before a drop at −3–27 °C corresponding to glass-rubber transition or energy dissipation during concomitant relaxation (Saïd Azizi Samir et al., 2004). At N-0, a hike post-relaxation was observed followed by 'plateau' indicating entangled nanofibers (M. Jonoobi et al., 2010; Saïd Azizi Samir et al., 2004), as confirmed morphologically (Fig. 3(a)). E' significantly increased by 104 % and 73 % at N-5 and even better at N-15 (161 % and 115 %) at 25 and 100 °C, respectively. These evidenced the enhanced heat stability and incorporated rigidity due to stronger interfacial interactions post-homogenization, on par with values of previous CNF reports (Gong et al., 2011; Ilyas et al., 2018; M. Jonoobi et al., 2010; Saba et al., 2017). The plateau faded due to promoted fibrillation and less tangling post-homogenization. However, despite still producing a higher thermal resistance than control, over-shearing at N-25 dramatically shortened the fibrils, making it highly prone to aggregation or agglomeration, hence the plateau reappearance. The next trait is E" that represents viscous response by measuring energy loss under stress or deformation as heat/cycle, associated with internal friction (Jawaid et al., 2015; Saba et al., 2017). A pattern similar to E' is found in E" plots (Fig. 7(b)) (Ilyas et al., 2018). Compared to control, E" of N-5 rose by 102 % and 64 %, and even higher at N-20 with a 180 % and 93 % increase at 25 and 100 °C, respectively, superior to those of other nanocellulose studies (Ilyas et al., 2018; Saba et al., 2017). Higher E" values emphasized a homogenous dispersion/distribution and less agglomeration (Saba et al., 2017; Xu et al., 2013). Lastly, Tan(δ) (Fig. 7 (c)) measures E" to E' ratio and characterizes recoverable strain energy in the distorted specimen, implying internal energy dissipation when exposed to varying temperatures (Sanyang et al., 2016). As the temperature increases, Tan(δ) increases to its maximum in the transition region and decreases in the rubbery region. A more intense peak means more molecular mobility, faster energy dissipation, and better dispersion, which inhibits movement. Whereas, agglomeration increases vacant space for the chain to move/rotate, thereby increasing visco-elastic behavior (Chen et al., 2008; Saba et al., 2017). The increase in E' and Tan(δ) can be attributed to the promoted interaction that restricts the segmental chain mobility, as usually aligned with mechanical properties (Fig. 6), where the reinforcing effect restricted molecular

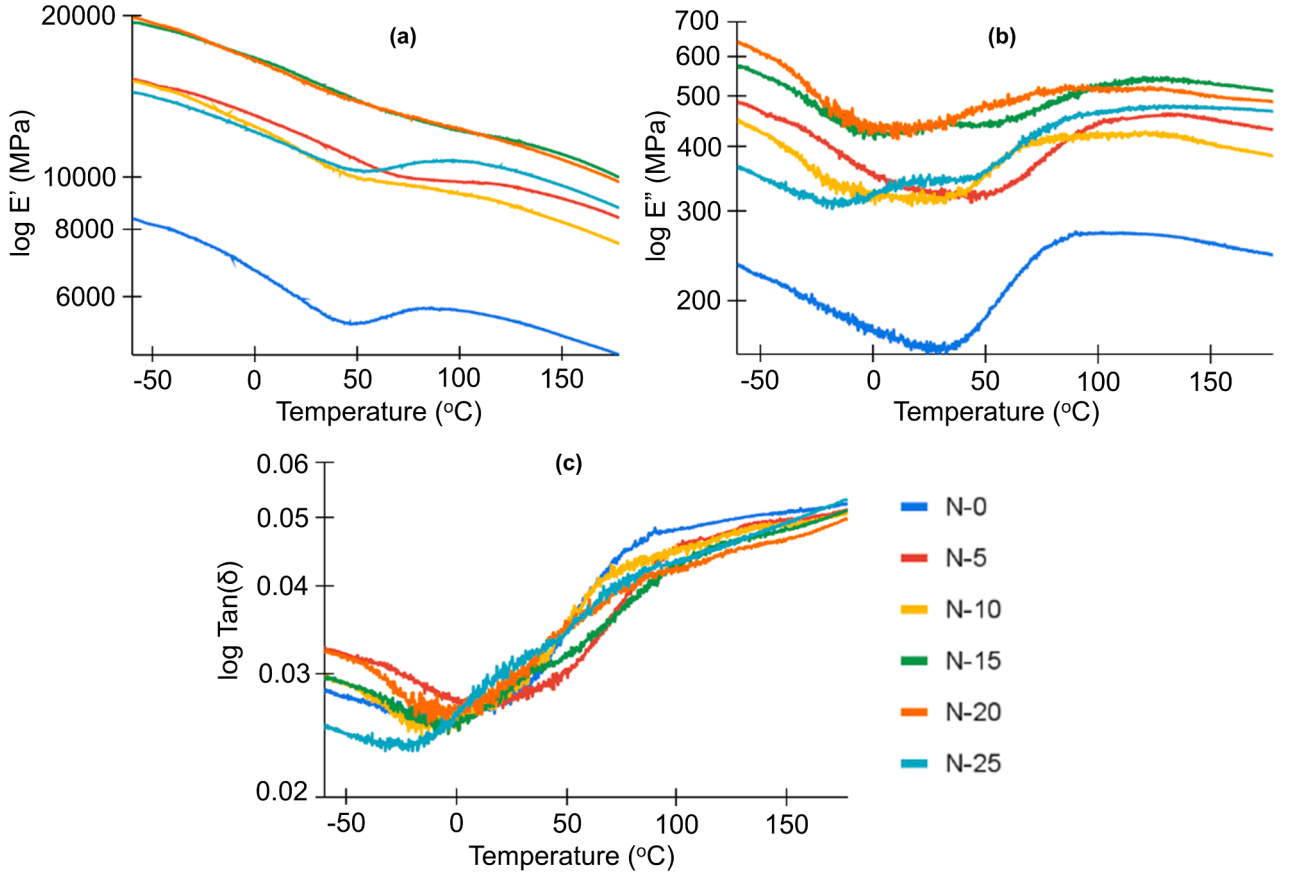

Fig. 7. DMA spectra of CNFs: (**a**) E', (**b**) E", (**c**) Tan(δ).

chain mobility (Bondeson et al., 2007; M. Jonoobi et al., 2010). These theories supported this work's findings, where N-0 showed the highest Tan(δ) at high temperatures (~70–100 °C) indicating the most molecular chain mobility by the untreated CNFs that consisted of bundles of entangled fibrils. As the fibrillation was enhanced post-homogenization, there became less moving space for the polymer chains as also confirmed morphologically (Fig. 3(a)). A significant decrease of 5 % and 10 % were observed at N-5 and N-25, respectively. These results are comparable to other reports (Gong et al., 2011; Ilyas et al., 2018; M. Jonoobi et al., 2010; Saba et al., 2017).

Fig. 8 and **Table S2** display the thermogravimetric analysis (TGA) results. CNFs typically begin to decompose through evaporation or dehydration at 40–47 °C due to the loosely bound moisture content. However, as freeze-dried CNF was used, the first decomposition was not initiated until water boiling point at 100 °C (Ilyas et al., 2018; Yang et al., 2019) (Fig. 8(a)). N-0 decomposed the earliest due to its still-natural high hydrophilicity (Abral et al., 2020), to be discussed further in the next section on contact angle (Fig. 9). The second significant weight loss was by cellulose decomposition through pyrolysis at 260–360 °C (Abral et al., 2019; Araújo et al., 2018), followed by the third after 360 °C attributing to the final, thermal-oxidative decomposition of char/ash (Asrofi et al., 2018; Zhao et al., 2013). An improvement in thermal resistance post-homogenization was evident, where CNFs managed to maintain 8–12 % of their initial weight and did not fully degrade even after reaching 700 °C (Fig. 8(b)), owing to the enhanced interlinking hydrogen bonding and energy requirement for decomposition (Islam et al., 2014; Kim et al., 2010). Temperature when the samples reached 5 % degradation ($T_{d,5\ \%}$, Fig. 8(c)) was enhanced by over 10 % post-homogenization, as similarly investigated in other studies (Fukuzumi et al., 2010; Supian et al., 2020; Yang et al., 2019). For heat-resistant applications, the recommended ambient temperature should not exceed 250 °C to ensure fit-for-use strength retention, therefore the obtained CNFs would suffice (Yang et al., 2019). Such thermostable films exhibit potential as conducting films in touch panels, displays, lighting devices, flexible printed circuit boards, solar cells, and medical devices (Sun et al., 2023). Thermal resistance could also be vital in (reheatable) food packaging applications (Abral et al., 2020; Ahmadzadeh et al., 2015; Fernandes et al., 2014; Van Nguyen et al., 2024).

3.8. *Contact angle*

Fig. 9 and **Table S3** showcases contact angle of CNF films. As previously mentioned in surface roughness discussion (Fig. 3(b)), the used solvent casting method caused a variance in microstructure, porosity, and pore size between the films' top and bottom surface, where the top tends to be significantly less hydrophilic (Jagodzińska et al., 2021; McGaughey et al., 2020). The more passes of homogenization, the higher the contact angle (or the lower the wettability/hydrophilicity). The highest contact angle was performed by N-25 regardless of the side of the film, a comparable result to previous reports (M. Jonoobi et al., 2010). Though surface roughness is among the crucial factors (M. Jonoobi et al., 2010), cellulose's naturally high hydrophilicity, meaning the plentiful polar groups (e.g., −OH, −COOH) (Q. Wang et al., 2018), was also taken into account. Studies have also proven a negative relationship between the number of polar functional groups and contact angle (Sun et al., 2021; Zhou et al., 2015). Hence, despite its roughest surface (Fig. 3(b)), N-0 did not display the highest contact angle. N-5, being the most hydrophilic, aligned with its surface being the smoothest. Regarding applicability, the less hydrophilic CNFs fit best as coating (Huang et al., 2022), while more hydrophilic ones would be suitable for hydrogel/aerogel as a drug-delivery system (De France et al., 2017). The

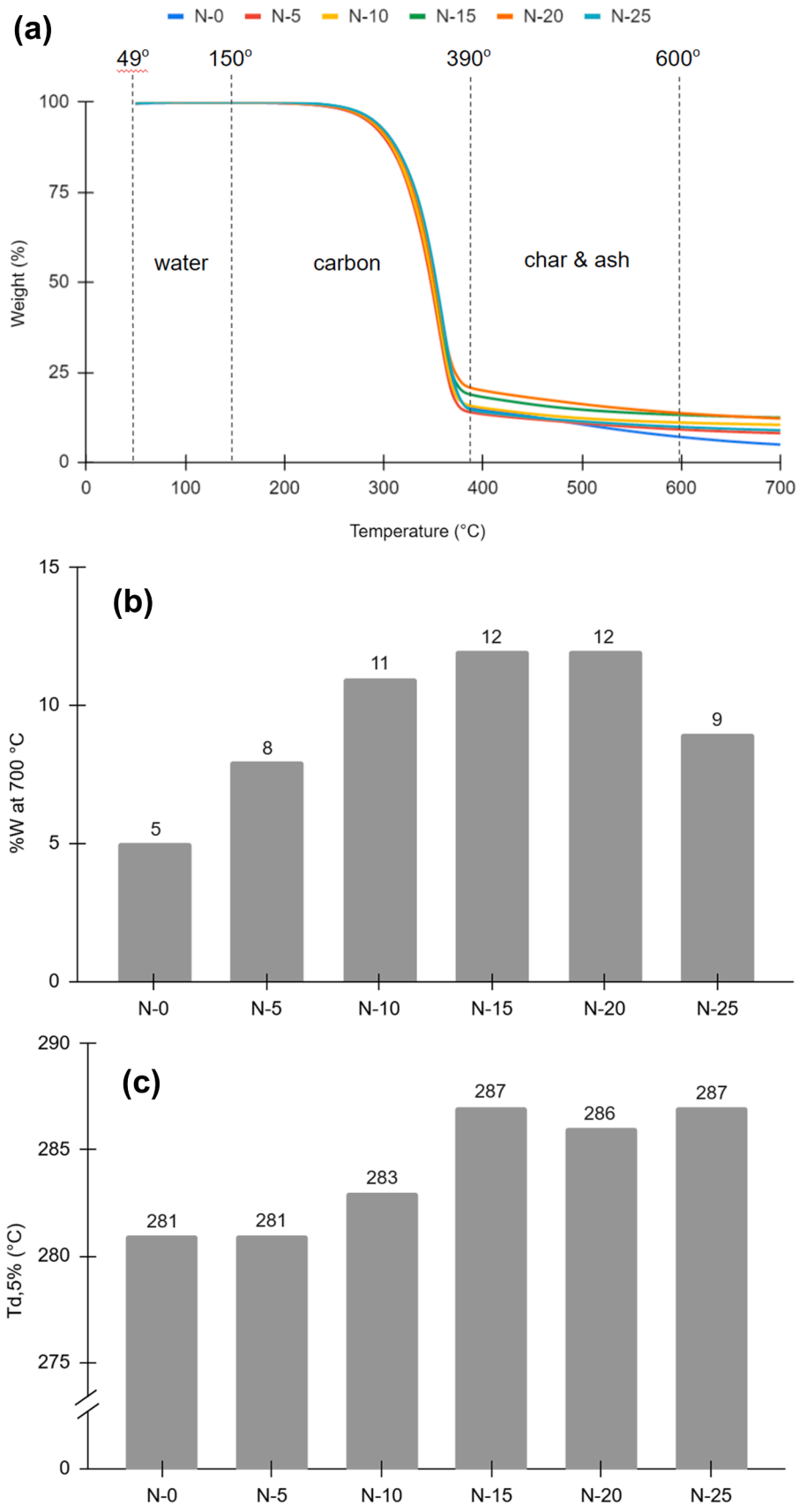

Fig. 8. (**a**) TGA spectra, (**b**) $T_{d,5\ \%}$, (**c**) %-weight at 700 °C of CNFs.

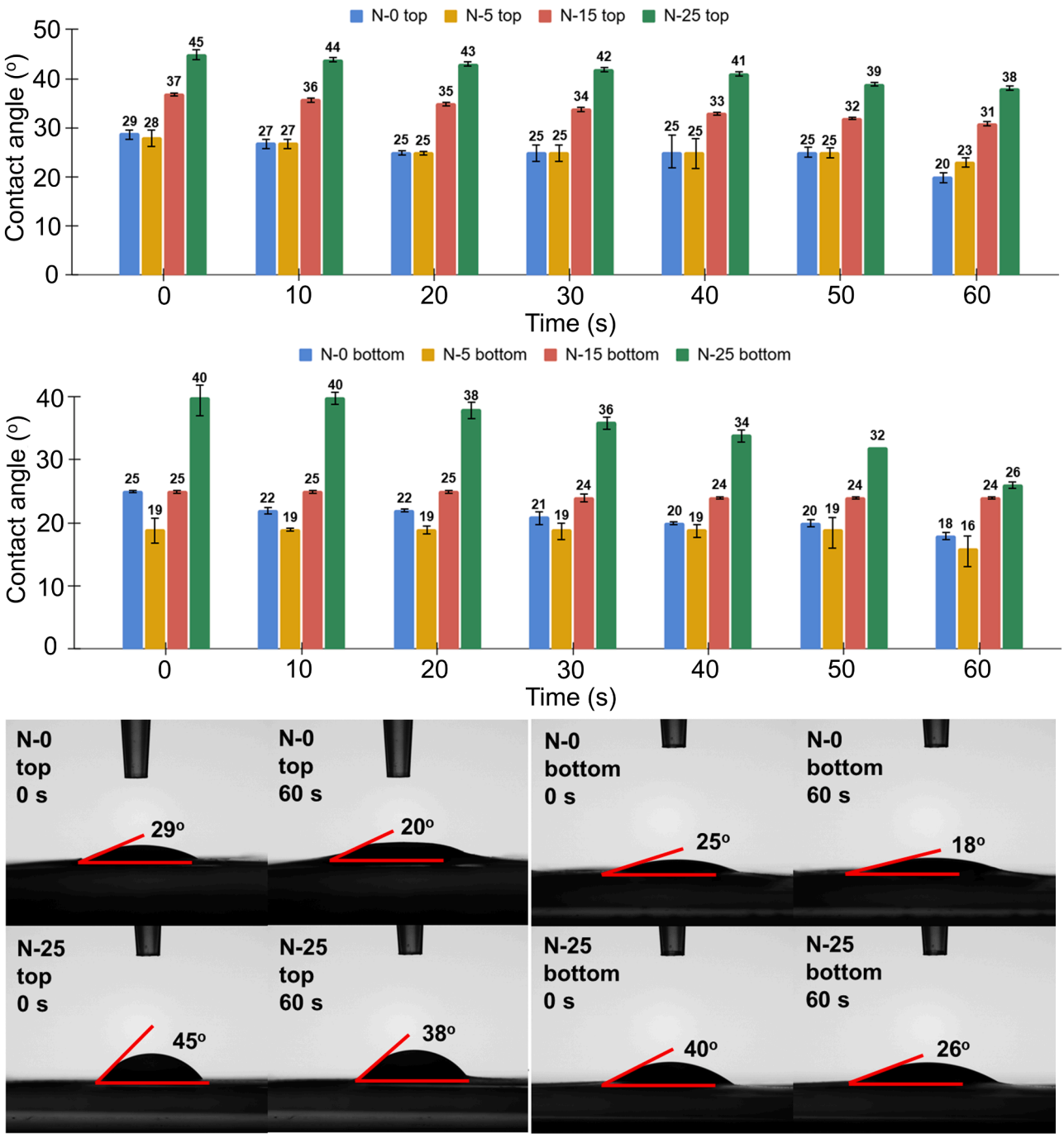

Fig. 9. Contact angle of CNF film's surface.

influence of film wettability in the food packaging field has been investigated (Asim et al., 2022; Balasubramaniam et al., 2020; Deng et al., 2017).

4. Conclusions

This work's findings comprehensively investigated and confirmed the significant advantages of the novel approach of low-pressure, multi-cycled homogenization on CNFs' fibrillation and the subsequent hydrogen bonding, promoting several functional properties, i.e., surface smoothness, oxygen permeability (comparable to commercial oxygen barrier resins like EVOH), mechanical properties, thermal properties, contact angle, on top of the successfully-maintained high crystallinity. The simplicity and mild operating condition of low pressure overcame the conventional, high-pressure homogenization techniques' recurring complications, particularly clogging, high cost/energy requirement, and molecular destruction. As the optimum number of homogenization cycles differs per property, further development can be designed according to the intended applications.

CRediT authorship contribution statement

Belladini Lovely: Writing – review & editing, Writing – original draft, Visualization, Validation, Software, Methodology, Investigation, Formal analysis, Data curation. **Young-Teck Kim:** Writing – review & editing, Validation, Resources, Project administration, Methodology, Formal analysis, Conceptualization. **Haibo Huang:** Writing – review & editing, Supervision, Funding acquisition, Formal analysis. **Audrey**

Zink-Sharp: Writing – review & editing, Methodology, Formal analysis. **Maren Roman:** Writing – review & editing, Methodology, Formal analysis.

Declaration of competing interest

The authors declare the following financial interests/personal relationships which may be considered as potential competing interests:

Young Teck Kim reports financial support was provided by USDA. If there are other authors, they declare that they have no known competing financial interests or personal relationships that could have appeared to influence the work reported in this paper.

Acknowledgements

This work is funded by the USDA–NIFA grant #2021–67017–33345 and made possible by the use of the VT Materials Characterization Facility (Institute for Critical Technology and Applied Science (ICTAS), Macromolecules Innovation Institute, Office of the Vice President for Research and Innovation) and instrumental facilities of Dr. Charles Frazier (VT Sustainable Biomaterials), Dr. Yifan Cheng (VT Food Science and Technology), and Dr. Robert Moore (VT Chemistry). Author Lovely also thanks Fulbright as her PhD sponsor.

Supplementary materials

Supplementary material associated with this article can be found, in the online version, at doi:10.1016/j.carpta.2025.100739.

Data availability

Data will be made available on request.

References

Abdelwahed, W., Degobert, G., Stainmesse, S., & Fessi, H. (2006). Freeze-drying of nanoparticles: formulation, process and storage considerations. *Advanced Drug Delivery Reviews, 58*, 1688–1713.

Abral, H., Ariksa, J., Mahardika, M., Handayani, D., Aminah, I., Sandrawati, N., Sugiarti, E., Muslimin, A. N., & Rosanti, S. D. (2020). Effect of heat treatment on thermal resistance, transparency and antimicrobial activity of sonicated ginger cellulose film. *Carbohydrate Polymers, 240*, Article 116287.

Abral, H., Basri, A., Muhammad, F., Fernando, Y., Hafizulhaq, F., Mahardika, M., Sugiarti, E., Sapuan, S. M., Ilyas, R. A., & Stephane, I. (2019). A simple method for improving the properties of the sago starch films prepared by using ultrasonication treatment. *Food Hydrocoll, 93*, 276–283.

Adamčík, L., Dzurenda, L., Banski, A., & Kminiak, R. (2023). Comparison of surface roughness of beech wood after sanding with an eccentric and belt sander. *Forests, Trees and Livelihoods, 15*, 45.

Aguayo, E., Tarazona-Díaz, M. P., Martínez-Sánchez, A., & García-González, A. (2017). Influence of moderate high-pressure homogenization on quality of bioactive compounds of functional food supplements. *Journal of Food Quality, 2017*.

Ahmadzadeh, S., Nasirpour, A., Keramat, J., Hamdami, N., Behzad, T., & Desobry, S. (2015). Nanoporous cellulose nanocomposite foams as high insulated food packaging materials. *Colloids and Surfaces A: Physicochemical and Engineering Aspects, 468*, 201–210.

Akerholm, M., Hinterstoisser, B., & Salmén, L. (2004). Characterization of the crystalline structure of cellulose using static and dynamic FT-IR spectroscopy. *Carbohydrate Research, 339*, 569–578.

E. Almenar, Minding the gap: Consumer awareness of packaging & food waste reduction, 2023.

Amini, E., Hafez, I., Tajvidi, M., & Bousfield, D. W. (2020). Cellulose and lignocellulose nanofibril suspensions and films: A comparison. *Carbohydrate Polymers, 250*, Article 117011.

Araújo, I. M. S., Silva, R. R., Pacheco, G., Lustri, W. R., Tercjak, A., Gutierrez, J., Júnior, J. R. S., Azevedo, F. H. C., Figuêredo, G. S., Vega, M. L., Ribeiro, S. J. L., & Barud, H. S. (2018). Hydrothermal synthesis of bacterial cellulose-copper oxide nanocomposites and evaluation of their antimicrobial activity. *Carbohydrate Polymers, 179*, 341–349.

Artzi, N., Narkis, M., & Siegmann, A. (2005). Review of melt-processed nanocomposites based on EVOH/organoclay. *Journal of Polymer Science Part B: Polymer Physics, 43*, 1931–1943.

Arun, R., Shruthy, R., Preetha, R., & Sreejit, V. (2022). Biodegradable nano composite reinforced with cellulose nano fiber from coconut industry waste for replacing synthetic plastic food packaging. *Chemosphere, 291*, Article 132786.

Asim, N., Badiei, M., & Mohammad, M. (2022). Recent advances in cellulose-based hydrophobic food packaging. *Emergent Mater, 5*, 703–718.

Asrofi, M., Abral, H., Kasim, A., Pratoto, A., Mahardika, M., & Hafizulhaq, F. (2018). Mechanical Properties of a Water Hyacinth Nanofiber Cellulose Reinforced Thermoplastic Starch Bionanocomposite: Effect of Ultrasonic Vibration during Processing. *Fibers and Polymers, 6*, 40.

ASTM, ASTM D638-14: Standard test method for tensile properties of plastics, 2022.

Atiqah, M. S. N., Gopakumar, D. A., O, F A T, Pottathara, Y. B., Rizal, S., Aprilia, N. A. S., Hermawan, D., Paridah, M. T. T., Thomas, S., & AK, H P S (2019). Extraction of cellulose Nanofibers via eco-friendly supercritical carbon dioxide treatment followed by mild acid hydrolysis and the fabrication of cellulose nanopapers. *Polymers, 11*.

Aulin, C., Gällstedt, M., & Lindström, T. (2010). Oxygen and oil barrier properties of microfibrillated cellulose films and coatings. *Cellulose, 17*, 559–574.

Ayranci, E., & Tunc, S. (2003). A method for the measurement of the oxygen permeability and the development of edible films to reduce the rate of oxidative reactions in fresh foods. *Food Chemistry, 80*, 423–431.

Babaee, M., Jonoobi, M., Hamzeh, Y., & Ashori, A. (2015). Biodegradability and mechanical properties of reinforced starch nanocomposites using cellulose nanofibers. *Carbohydrate Polymers, 132*, 1–8.

Balasubramaniam, S. L., Patel, A. S., & Nayak, B. (2020). Surface modification of cellulose nanofiber film with fatty acids for developing renewable hydrophobic food packaging. *Food Packag. Shelf Life, 26*, Article 100587.

Birkett, G. C., Sicoli, S., Horvath, L., Foster, J., Kim, Y.-T., Renneckar, S., & Goodell, B. (2017). Investigation of nanofibrillated cellulose for hydrophobic packaging material: Examining alternatives to solvent exchange and lyophilization. *BioResources, 12*, 4314–4326.

Bondeson, D., Syre, P., & Niska, K. O. (2007). All cellulose nanocomposites produced by extrusion. *Journal of Biobased Materials and Bioenergy, 1*, 367–371.

Boulemkahel, S., Betoret, E., Benatallah, L., & Rosell, C. M. (2021). Effect of low pressures homogenization on the physico-chemical and functional properties of rice flour. *Food Hydrocoll, 112*, Article 106373.

Brown, N. (1992). *Plastics in Food Patkaging: Properties: Design and Fabrication*. CRC Press.

Byun, Y., Rodriguez, K., Han, J. H., & Kim, Y. T. (2015). Improved thermal stability of polylactic acid (PLA) composite film via PLA-β-cyclodextrin-inclusion complex systems. *International Journal of Biological Macromolecules, 81*, 591–598.

Candan, Z., Gardner, D. J., & Shaler, S. M. (2016). Dynamic mechanical thermal analysis (DMTA) of cellulose nanofibril/nanoclay/pMDI nanocomposites. *Composites Part B Engineering, 90*, 126–132.

Charles, D., & Kimman, L. (2023). *Plastic Waste Makers Index 2023*.

Chen, G., Wei, M., Chen, J., Huang, J., Dufresne, A., & Chang, P. R. (2008). Simultaneous reinforcing and toughening: New nanocomposites of waterborne polyurethane filled with low loading level of starch nanocrystals, simultaneous reinforcing and toughening: new nanocomposites of waterborne polyurethane filled with low loading level of starch nanocrystals. *Polymer, 7*, 1860–1870.

Chen, G., Zhang, B., Zhao, J., & Chen, H. (2014). Development and characterization of food packaging film from cellulose sulfate. *Food Hydrocoll, 35*, 476–483.

Cheng, Q., & Via, B. (2017). Characterization of cellulose fibril aggregates isolated by the combination of ultrasonication and homogenizer. *Wood Material Science and Engineering, 12*, 197–202.

Cheng, S., Zhang, Y., Cha, R., Yang, J., & Jiang, X. (2015). Water-soluble nanocrystalline cellulose films with highly transparent and oxygen barrier properties. *Nanoscale, 8*, 973–978.

Cheng, W., Chen, J., Liu, D., Ye, X., & Ke, F. (2010). Impact of ultrasonic treatment on properties of starch film-forming dispersion and the resulting films. *Carbohydrate Polymers, 81*, 707–711.

Chinga-Carrasco, G., Averianova, N., Kondalenko, O., Garaeva, M., Petrov, V., Leinsvang, B., & Karlsen, T. (2014). The effect of residual fibres on the micro-topography of cellulose nanopaper. *Micron (Oxford, England: 1993), 56*, 80–84.

Chun, S.-J., Lee, S.-Y., Doh, G.-H., Lee, S., & Kim, J. H. (2011). Preparation of ultrastrength nanopapers using cellulose nanofibrils. *Journal of Industrial and Engineering Chemistry, 17*, 521–526.

Daicho, K., Saito, T., Fujisawa, S., & Isogai, A. (2018). The crystallinity of nanocellulose: Dispersion-induced disordering of the grain boundary in biologically structured cellulose. *ACS Applied Nano Materials, 1*, 5774–5785.

Davoudpour, Y., Hossain, S., Khalil, H. P. S. A., Haafiz, M. K. M., Ishak, Z. A. M., Hassan, A., & Sarker, Z. I. (2015). Optimization of high pressure homogenization parameters for the isolation of cellulosic nanofibers using response surface methodology. *Industrial Crops and Products, 74*, 381–387.

De France, K. J., Hoare, T., & Cranston, E. D. (2017). Review of hydrogels and aerogels containing nanocellulose. *Chemistry of Materials, 29*, 4609–4631.

Deng, Z., Jung, J., & Zhao, Y. (2017). Development, characterization, and validation of chitosan adsorbed cellulose nanofiber (CNF) films as water resistant and antibacterial food contact packaging. *Food Science and Technology, 83*, 132–140.

Dias, O. A. T., Konar, S., Leão, A. L., Yang, W., Tjong, J., & Sain, M. (2020). Current state of applications of nanocellulose in flexible energy and electronic devices. *Frontiers in Chemistry, 8*, 420.

Dilamian, M., & Noroozi, B. (2019). A combined homogenization-high intensity ultrasonication process for individualizaion of cellulose micro-nano fibers from rice straw. *Cellulose, 26*, 5831–5849.

Dinesh, G., & Kandasubramanian, B. (2022). Fabrication of transparent paper devices from nanocellulose fiber. *Materials Chemistry and Physics, 281*, Article 125707.

Djafari Petroudy, S. R. (2017). 3 - Physical and mechanical properties of natural fibers (Eds.). In M. Fan, & F. Fu (Eds.), *Advanced High Strength Natural Fibre Composites in Construction* (pp. 59–83). Woodhead Publishing.

Doebelin, N., & Kleeberg, R. (2015). Profex: a graphical user interface for the rietveld refinement program BGMN. *Journal of Applied Crystallography, 48*, 1573–1580.

Dogan, N., & McHugh, T. H. (2007). Effects of microcrystalline cellulose on functional properties of hydroxy propyl methyl cellulose microcomposite films. *Journal of Food Science, 72*, E016–E022.
Du, C., Li, H., Li, B., Liu, M., & Zhan, H. (2016). Characteristics and properties of cellulose nanofibers prepared by TEMPO oxidation of corn husk. *BioResources, 11*, 5276–5284.
EPA, Reducing wasted food and packaging: a guide for food services and restaurants, (2015).
EPA, International efforts on wasted food recovery, (2016).
Etale, A., Onyianta, A. J., Turner, S. R., & Eichhorn, S. J. (2023). Cellulose: A review of water interactions, applications in composites, and water treatment. *Chem. Rev., 123*, 2016–2048.
European Commission. (2023). *Waste Framework Directive*.
FAO, Food Wastage Footprint: Impacts on Natural Resources: Summary Report, (2013).
FAO, Food waste FAQs, Https://www.usda.gov/foodwaste/faqs (2021).
FAO, Voluntary code of conduct for food loss and waste reduction, (2022).
Fein, K., Bousfield, D. W., & Gramlich, W. M. (2021). Processing effects on structure, strength, and barrier properties of refiner-produced cellulose nanofibril layers. *ACS Applied Polymer Materials, 3*, 3666–3678.
Fernandes, S. C. M., Sadocco, P., Causio, J., Silvestre, A. J. D., Mondragon, I., & Freire, C. S. R. (2014). Antimicrobial pullulan derivative prepared by grafting with 3-aminopropyltrimethoxysilane: Characterization and ability to form transparent films. *Food Hydrocoll, 35*, 247–252.
Flores, Z., San-Martin, D., Beldarraín-Iznaga, T., Leiva-Vega, J., & Villalobos-Carvajal, R. (2021). Effect of homogenization method and carvacrol content on microstructural and physical properties of chitosan-based films. *Foods, 10*.
Fu, Z.-Q., Wang, L.-J., Li, D., Wei, Q., & Adhikari, B. (2011). Effects of high-pressure homogenization on the properties of starch-plasticizer dispersions and their films. *Carbohydrate Polymers, 86*, 202–207.
Fukuzumi, H., Fujisawa, S., Saito, T., & Isogai, A. (2013). Selective permeation of hydrogen gas using cellulose nanofibril film. *Biomacromolecules, 14*, 1705–1709.
Fukuzumi, H., Saito, T., Iwata, T., Kumamoto, Y., & Isogai, A. (2009). Transparent and high gas barrier films of cellulose nanofibers prepared by TEMPO-mediated oxidation. *Biomacromolecules, 10*, 162–165.
Fukuzumi, H., Saito, T., Okita, Y., & Isogai, A. (2010). Thermal stabilization of TEMPO-oxidized cellulose. *Polymer Degradation and Stability, 95*, 1502–1508.
Geyer, R., Jambeck, J. R., & Law, K. L. (2017). Production, use, and fate of all plastics ever made. *Science Advances, 3*, Article e1700782.
Gong, G., Pyo, J., Mathew, A. P., & Oksman, K. (2011). Tensile behavior, morphology and viscoelastic analysis of cellulose nanofiber-reinforced (CNF) polyvinyl acetate (PVAc). *Composites - Part A: Applied Science and Manufacturing, 42*, 1275–1282.
Guo, Z., Zhao, B., Chen, L., & Zheng, B. (2019). Physicochemical properties and digestion of lotus seed starch under high-pressure homogenization. *Nutrients, 11*.
Hafez, I., Amini, E., & Tajvidi, M. (2020). The synergy between cellulose nanofibrils and calcium carbonate in a hybrid composite system. *Cellulose, 27*, 3773–3787.
Han, J., Chen, M., Liu, H., Zhang, D., Shi, Q.-S., Xie, X., & Guo, Y. (2024). Antimicrobial and degradable all-cellulose composite for functional and sustainable food packaging. *Industrial Crops and Products, 222*, Article 119966.
Herrera, M. (2015). Preparation and characterization of nanocellulose films and coatings from industrial bio-residues. *Luleå Tekniska Universitet*.
Herrera, M. A., Mathew, A. P., & Oksman, K. (2012). Comparison of cellulose nanowhiskers extracted from industrial bio-residue and commercial microcrystalline cellulose. *Materials Letters, 71*, 28–31.
F.W. Herrick, R.L. Casebier, J. Hamilton, K.R. Sandberg, Microfibrillated cellulose: morphology and accessibility, https://www.semanticscholar.org ⟩ Paper ⟩ Microfibrillat...https://www.semanticscholar.org ⟩ Paper ⟩ Microfibrillat... (1983).
Hong, S.-I., & Krochta, J. M. (2006). Oxygen barrier performance of whey-protein-coated plastic films as affected by temperature, relative humidity, base film and protein type. *Journal of Food Engineering, 77*, 739–745.
Hoover, R., & Ratnayake, W. S. (2002). Starch characteristics of black bean, chick pea, lentil, navy bean and pinto bean cultivars grown in Canada. *Food Chemistry, 78*, 489–498.
Huang, D., Wu, M., Wang, C., Kuga, S., & Huang, Y. (2020). Effect of partial dehydration on freeze-drying of aqueous nanocellulose suspension. *ACS Sustainable Chemistry & Engineering, 8*, 11389–11395.
Huang, K., & Wang, Y. (2022). Recent applications of regenerated cellulose films and hydrogels in food packaging. *Current Opinion in Food Science, 43*, 7–17.
Huang, S., Wang, X., Zhang, Y., Meng, Y., Hua, F., & Xia, X. (2022). Cellulose nanofibers/polyvinyl alcohol blends as an efficient coating to improve the hydrophobic and oleophobic properties of paper. *Scientific Reports, 12*, 1–10.
Ibrahim, H., Sazali, N., Ibrahim, I. N., & Sharip, M. S. (2019). Nano-structured cellulose as green adsorbents for water purification: A mini review. *Amstelodamum, 23*.
Ilyas, R. A., Sapuan, S. M., Ishak, M. R., & Zainudin, E. S. (2018). Development and characterization of sugar palm nanocrystalline cellulose reinforced sugar palm starch bionanocomposites. *Carbohydrate Polymers, 202*, 186–202.
Ilyas, R. A., Sapuan, S. M., Ishak, M. R., & Zainudin, E. S. (2019). Sugar palm nanofibrillated cellulose (Arenga pinnata (Wurmb.) Merr): Effect of cycles on their yield, physic-chemical, morphological and thermal behavior. *International Journal of Biological Macromolecules, 123*, 379–388.
Islam, A., Yasin, T., & ur Rehman, I. (2014). Synthesis of hybrid polymer networks of irradiated chitosan/poly(vinyl alcohol) for biomedical applications. *Radiation Physics and Chemistry, 96*, 115–119.
Iwamoto, S., Nakagaito, A. N., & Yano, H. (2007). Nano-fibrillation of pulp fibers for the processing of transparent nanocomposites. *Applied Physics A: Materials Science and Processing, 89*, 461–466.
Jagodzińska, S., Research Network Łukasiewicz - Institute of Biopolymers and Chemical Fibres, Pałys, B., & Wawro, D. (2021). Institute of security technologies "MORATEX," Effect of chitosan film surface structure on the contact angle. *Progress on Chemistry and Application of Chitin and its Derivatives, 26*, 89–100.
Jain, P. K., Pandey, P. M., & Rao, P. V. M. (2009). Selective laser sintering of clay-reinforced polyamide. *Polymer Composites*. NA–NA.
Jawaid, M., Alothman, O. Y., Saba, N., Tahir, P. M., & Khalil, H. P. S. A. (2015). Effect of fibers treatment on dynamic mechanical and thermal properties of epoxy hybrid composites. *Polymer Composites, 36*, 1669–1674.
Jonoobi, M., Harun, J., Mathew, A. P., Hussein, M. Z. B., & Oksman, K. (2010). Preparation of cellulose nanofibers with hydrophobic surface characteristics. *Cellulose, 17*, 299–307.
Jonoobi, M., Harun, J., Mathew, A. P., & Oksman, K. (2010). Mechanical properties of cellulose nanofiber (CNF) reinforced polylactic acid (PLA) prepared by twin screw extrusion. *Composites Science and Technology, 70*, 1742–1747.
Josset, S., Orsolini, P., Siqueira, G., Tejado, A., Tingaut, P., & Zimmermann, T. (2014). Energy consumption of the nanofibrillation of bleached pulp, wheat straw and recycled newspaper through a grinding process. *Nordic Pulp & Paper Research Journal, 29*, 167–175.
Jurowski, K., & Grzeszczyk, S. (2015). The influence of concrete composition on Young's modulus. *Procedia Engineering, 108*, 584–591.
Kalia, S., Boufi, S., Celli, A., & Kango, S. (2014). Nanofibrillated cellulose: surface modification and potential applications. *Colloid and Polymer Science, 292*, 5–31.
Kasemwong, K., Ruktanonchai, U. R., Srinuanchai, W., Itthisoponkul, T., & Sriroth, K. (2011). Effect of high-pressure microfluidization on the structure of cassava starch granule. *Starke, 63*, 160–170.
Keyence, Contact-type surface Roughness/profile measuring instruments, (2021).
Kim, U.-J., Eom, S. H., & Wada, M. (2010). Thermal decomposition of native cellulose: Influence on crystallite size. *Polymer Degradation and Stability, 95*, 778–781.
Kittle, J. D., Qian, C., Edgar, E., Roman, M., & Esker, A. R. (2018). Adsorption of xyloglucan onto thin films of cellulose nanocrystals and amorphous cellulose: Film thickness effects. *ACS Omega, 3*, 14004–14012.
Klemm, D., Philipp, B., Heinze, T., Heinze, U., Wagenknecht, W., & Comprehensive Cellulose Chemistry. (1998). *Comprehensive Cellulose Chemistry: Fundamentals and Analytical Methods,*. Wiley.
Koontz, J. L. (2016). Chapter 13 - Packaging Technologies to Control Lipid Oxidation. In M. Hu, & C. Jacobsen (Eds.), *Oxidative Stability and Shelf Life of Foods Containing Oils and Fats* (pp. 479–517). AOCS Press.
Korhonen, J. T., Kettunen, M., Ras, R. H. A., & Ikkala, O. (2011). Hydrophobic nanocellulose aerogels as floating, sustainable, reusable, and recyclable oil absorbents. *ACS Appl Mater Interfaces, 3*, 1813–1816.
Kose, R., Mitani, I., Kasai, W., & Kondo, T. (2011). Nanocellulose" as a single nanofiber prepared from pellicle secreted by Gluconacetobacter xylinus using aqueous counter collision. *Biomacromolecules, 12*, 716–720.
Kourkoumelis, N., & PowDLL, a reusable. (2013). NET component for interconverting powder diffraction data: Recent developments. *Powder Diffraction, 28*, 137–148.
Kumar, V., Bollström, R., Yang, A., Chen, Q., Chen, G., Salminen, P., Bousfield, D., & Toivakka, M. (2014). Comparison of nano- and microfibrillated cellulose films. *Cellulose, 21*, 3443–3456.
Kuraray, Oxygen barrier, (1972).
Kwan, K. S. (1998). *The role of penetrant structure in the transport and mechanical properties of a thermoset adhesive*. Virginia Polytechnic Institute and State University.
Lavoine, N., Desloges, I., Dufresne, A., & Bras, J. (2012). Microfibrillated cellulose - its barrier properties and applications in cellulosic materials: a review. *Carbohydrate Polymers, 90*, 735–764.
Lee, H., Sundaram, J., & Mani, S. (2017). Production of cellulose nanofibrils and their application to food: A review. In R. Prasad, V. Kumar, & M. Kumar (Eds.), *Nanotechnology: Food and Environmental Paradigm* (pp. 1–33). Singapore: Springer Singapore.
Lee, J.-C., Lee, J.-A., Lim, D.-Y., & Kim, K.-Y. (2018). Fabrication of Cellulose Nanofiber Reinforced Thermoplastic Composites. *Fibers and Polymers, 19*, 1753–1759.
Lee, J. T. Y., & Chow, K. L. (2012). SEM sample preparation for cells on 3D scaffolds by freeze-drying and HMDS: SEM sample preparation for cells. *Scanning, 34*, 12–25.
Lehmann, D., & Zahn, D. R. T. (2009). The electrical and dielectrical behavior of n-conducting perylene tetracarboxylic diimide derivatives. *Applied Physics A: Materials Science and Processing, 95*, 203–207.
Li, V. C. F., Mulyadi, A., Dunn, C. K., Deng, Y., & Qi, H. J. (2018). Direct ink write 3D printed cellulose nanofiber aerogel structures with highly deformable, shape recoverable, and functionalizable properties. *ACS Sustainable Chemistry & Engineering, 6*, 2011–2022.
Liu, A., Walther, A., Ikkala, O., Belova, L., & Berglund, L. A. (2011). Clay nanopaper with tough cellulose nanofiber matrix for fire retardancy and gas barrier functions. *Biomacromolecules, 12*, 633–641.
Liu, X., Sun, H., Mu, T., Fauconnier, M. L., & Li, M. (2023). Preparation of cellulose nanofibers from potato residues by ultrasonication combined with high-pressure homogenization. *Food Chemistry, 413*, Article 135675.
Liu, Y., Fu, H., Zhang, W., & Liu, H. (2022). Effect of crystalline structure on the catalytic hydrolysis of cellulose in subcritical water. *ACS Sustainable Chemistry & Engineering, 10*, 5859–5866.
Lizundia, E., Urruchi, A., Vilas, J. L., & León, L. M. (2016). Increased functional properties and thermal stability of flexible cellulose nanocrystal/ZnO films. *Carbohydrate Polymers, 136*, 250–258.
Lou, D., Grablander, T., Mao, M., Hong, H., & Peterson, G. P. (2021). Improved thermal conductivity of PEG-based fluids using hydrogen bonding and long chain of nanoparticle. *Journal of Nanoparticle Research, 23*, 98.
Magoulas, A. (2016). *Protecting Your Family from Food Spoilage*.

Malucelli, L. C., Matos, M., Jordão, C., Lacerda, L. G., Carvalho Filho, M. A. S., & Magalhães, W. L. E. (2018). Grinding severity influences the viscosity of cellulose nanofiber (CNF) suspensions and mechanical properties of nanopaper. *Cellulose, 25*, 6581–6589.
Manimaran, P., Saravanan, S. P., Sanjay, M. R., Siengchin, S., Jawaid, M., & Khan, A. (2019). Characterization of new cellulosic fiber: Dracaena reflexa as a reinforcement for polymer composite structures. *Journal of Materials Research and Technology, 8*, 1952–1963.
McGaughey, A. L., Karandikar, P., Gupta, M., & Childress, A. E. (2020). Hydrophobicity versus pore size: Polymer coatings to improve membrane wetting resistance for membrane distillation. *ACS Applied Polymer Materials, 2*, 1256–1267.
Meng, S., Ma, Y., Sun, D.-W., Wang, L., & Liu, T. (2014). Properties of starch-palmitic acid complexes prepared by high pressure homogenization. *Journal of Cereal Science, 59*, 25–32.
Michiels, Y., Van Puyvelde, P., & Sels, B. (2017). Barriers and chemistry in a bottle: Mechanisms in today's oxygen barriers for tomorrow's materials. *NATO Advanced Science Institutes Series E, 7*, 665.
Miettinen, A., Chinga-Carrasco, G., & Kataja, M. (2014). Three-dimensional microstructural properties of nanofibrillated cellulose films. *International Journal of Molecular Sciences, 15*, 6423–6440.
Mike. (2022). *Sa does not equal Ra!* Michigan Metrology.
Mokhena, T. C., Sadiku, E. R., Mochane, M. J., Ray, S. S., John, M. J., & Mtibe, A. (2021). Mechanical properties of cellulose nanofibril papers and their bionanocomposites: A review. *Carbohydrate Polymers, 273*, Article 118507.
Morán, J. I., Alvarez, V. A., Cyras, V. P., & Vázquez, A. (2008). Extraction of cellulose and preparation of nanocellulose from sisal fibers. *Cellulose, 15*, 149–159.
Naderi, A., Lindström, T., & Sundström, J. (2015). Repeated homogenization, a route for decreasing the energy consumption in the manufacturing process of carboxymethylated nanofibrillated cellulose? *Cellulose, 22*, 1147–1157.
Nagarajan, K. J., Ramanujam, N. R., Sanjay, M. R., Siengchin, S., Surya Rajan, B., Sathick Basha, K., Madhu, P., & Raghav, G. R. (2021). A comprehensive review on cellulose nanocrystals and cellulose nanofibers: Pretreatment, preparation, and characterization. *Polymer Composites, 42*, 1588–1630.
Nair, S. S., Zhu, J. Y., Deng, Y., & Ragauskas, A. J. (2014). High performance green barriers based on nanocellulose. *Sustainable Chemical Processes, 2*, 1–7.
Nakagaito, A. N., & Yano, H. (2004). The effect of morphological changes from pulp fiber towards nano-scale fibrillated cellulose on the mechanical properties of high-strength plant fiber based composites. *Applied Physics A: Materials Science and Processing, 78*, 547–552.
Nechyporchuk, O., Belgacem, M. N., & Bras, J. (2016). Production of cellulose nanofibrils: A review of recent advances. *Industrial Crops and Products, 93*, 2–25.
Niu, X., Huan, S., Li, H., Pan, H., & Rojas, O. J. (2021). Transparent films by ionic liquid welding of cellulose nanofibers and polylactide: Enhanced biodegradability in marine environments. *Journal of Hazardous Materials, 402*, Article 124073.
NRDC. (2020). *Composting, 101*.
Nurhadi, B., Angeline, A., Sukri, N., Masruchin, N., Arifin, H. R., & Saputra, R. A. (2022). Characteristics of microcrystalline cellulose from nata de coco: Hydrochloric acid versus maleic acid hydrolysis. *Journal of Applied Polymer Science, 139*, 51576.
Oms-Oliu, G., Soliva-Fortuny, R., & Martín-Belloso, O. (2008). Edible coatings with antibrowning agents to maintain sensory quality and antioxidant properties of fresh-cut pears. *Postharvest Biology and Technology, 50*, 87–94.
Osterberg, M., Vartiainen, J., Lucenius, J., Hippi, U., Seppälä, J., Serimaa, R., & Laine, J. (2013). A fast method to produce strong NFC films as a platform for barrier and functional materials. *ACS Appl Mater Interfaces, 5*, 4640–4647.
Palmkron, S. B., Bergenståhl, B., Håkansson, S., Wahlgren, M., Fureby, A. M., & Larsson, E. (2023). Quantification of structures in freeze-dried materials using X-ray microtomography. *Colloids and Surfaces A: Physicochemical and Engineering Aspects, 658*, Article 130726.
Park, S., Baker, J. O., Himmel, M. E., Parilla, P. A., & Johnson, D. K. (2010). Cellulose crystallinity index: measurement techniques and their impact on interpreting cellulase performance. *Biotechnology for Biofuels, 3*, 10.
Pavlík, Z., Pavlíková, M., & Záleská, M. (2019). 9 - Properties of concrete with plastic polypropylene aggregates. In F. Pacheco-Torgal, J. Khatib, F. Colangelo, & R. Tuladhar (Eds.), *Use of Recycled Plastics in Eco-Efficient Concrete* (pp. 189–213). Woodhead Publishing.
Pelissari, F. M., Andrade-Mahecha, M. M., do, P. J., Sobral, A., & Menegalli, F. C. (2017). Nanocomposites based on banana starch reinforced with cellulose nanofibers isolated from banana peels. *Journal of Colloid & Interface Science, 505*, 154–167.
Peresin, M. S., Kammiovirta, K., Heikkinen, H., Johansson, L.-S., Vartiainen, J., Setälä, H., Österberg, M., & Tammelin, T. (2017). Understanding the mechanisms of oxygen diffusion through surface functionalized nanocellulose films. *Carbohydrate Polymers, 174*, 309–317.
Pion, How BEE's emulsifying cell revolutionized the homogenizer, (2015).
Pion, The advantages of BEE brand homogenizers for cell lysis, (2024).
Quiévy, N., Jacquet, N., Sclavons, M., Deroanne, C., Paquot, M., & Devaux, J. (2010). Influence of homogenization and drying on the thermal stability of microfibrillated cellulose. *Polymer Degradation and Stability, 95*, 306–314.
Redlinger-Pohn, J. D., Petkovšek, M., Gordeyeva, K., Zupanc, M., Gordeeva, A., Zhang, Q., Dular, M., & Söderberg, L. D. (2022). Cavitation fibrillation of cellulose fiber. *Biomacromolecules, 23*, 847–862.
ReFED. (2018). In *2018 Retail food waste action guide*.
Roilo, D., Maestri, C. A., Scarpa, M., Bettotti, P., & Checchetto, R. (2018). Gas barrier and optical properties of cellulose nanofiber coatings with dispersed TiO2 nanoparticles. *Surface & Coatings Technology, 343*, 131–137.
Rojas-Graü, M. A., Tapia, M. S., Rodríguez, F. J., Carmona, A. J., & Martin-Belloso, O. (2007). Alginate and gellan-based edible coatings as carriers of antibrowning agents applied on fresh-cut Fuji apples. *Food Hydrocoll, 21*, 118–127.
Saba, N., Safwan, A., Sanyang, M. L., Mohammad, F., Pervaiz, M., Jawaid, M., Alothman, O. Y., & Sain, M. (2017). Thermal and dynamic mechanical properties of cellulose nanofibers reinforced epoxy composites. *International Journal of Biological Macromolecules, 102*, 822–828.
Saïd Azizi Samir, M. A., Alloin, F., Paillet, M., & Dufresne, A. (2004). Tangling effect in fibrillated cellulose reinforced nanocomposites. *Macromolecules, 37*, 4313–4316.
Sanyang, M. L., Sapuan, S. M., Jawaid, M., Ishak, M. R., & Sahari, J. (2016). Development and characterization of sugar palm starch and poly(lactic acid) bilayer films. *Carbohydrate Polymers, 146*, 36–45.
Schultz, T. P., McGinnis, G. D., & Bertran, M. S. (1985). Estimation of cellulose crystallinity using Fourier transform-infrared spectroscopy and dynamic thermogravimetry. *Journal of Wood Chemistry and Technology, 5*, 543–557.
Segal, L., Creely, J. J., Martin, A. E., & Conrad, C. M. (1959). An empirical method for estimating the degree of crystallinity of native cellulose using the X-ray diffractometer. *Textile Research Journal, 29*, 786–794.
Shamskar, K. Rahbar, Heidari, H., & Rashidi, A. (2019). Study on nanocellulose properties processed using different methods and their aerogels. *Journal of Polymers and the Environment, 27*, 1418–1428.
Siró, I., Plackett, D., Hedenqvist, M., Ankerfors, M., & Lindström, T. (2011). Highly transparent films from carboxymethylated microfibrillated cellulose: The effect of multiple homogenization steps on key properties. *Journal of Applied Polymer Science, 119*, 2652–2660.
Siti Syazwani, N., Ervina Efzan, M. N., Kok, C. K., & Nurhidayatullaili, M. J. (2022). Analysis on extracted jute cellulose nanofibers by Fourier transform infrared and X-Ray diffraction. *Journal of Building Engineering, 48*, Article 103744.
Sjostrom, E. (2013). *Wood Chemistry: Fundamentals and Applications*. San Diego, California: Elsevier.
Sluiter, A., Hames, B., Ruiz, R., Scarlata, C., Sluiter, J., Templeton, D., & Crocker, D. (2008). *Determination Structural Carbohydrates Lignin Biomass*. National Renewable Energy Laboratory.
Sofla, M. R. K., Brown, R. J., Tsuzuki, T., & Rainey, T. J. (2016). A comparison of cellulose nanocrystals and cellulose nanofibres extracted from bagasse using acid and ball milling methods. *Advances in Natural Sciences: Nanoscience and Nanotechnology, 7*, Article 035004.
Soni, B., Hassan, E. B., & Mahmoud, B. (2015). Chemical isolation and characterization of different cellulose nanofibers from cotton stalks. *Carbohydrate Polymers, 134*, 581–589.
Spence, K. L., Venditti, R. A., Habibi, Y., Rojas, O. J., & Pawlak, J. J. (2010). The effect of chemical composition on microfibrillar cellulose films from wood pulps: mechanical processing and physical properties. *Bioresource Technology, 101*, 5961–5968.
SriBala, G., Chennuru, R., Mahapatra, S., & Vinu, R. (2016). Effect of alkaline ultrasonic pretreatment on crystalline morphology and enzymatic hydrolysis of cellulose. *Cellulose, 23*, 1725–1740.
Stelte, W., & Sanadi, A. R. (2009). Preparation and Characterization of Cellulose Nanofibers from Two Commercial Hardwood and Softwood Pulps. *Industrial & Engineering Chemistry Research, 48*, 11211–11219.
Sun, L., Zhang, D., Cheng, S. Z. D., & Harris, F. W. (2023). Thermally stable transparent polymer films for flexible electronics: Properties and applications. *Giant, 14*, Article 100156.
Sun, X., Wu, Q., Picha, D. H., Ferguson, M. H., Ndukwe, I. E., & Azadi, P. (2021). Comparative performance of bio-based coatings formulated with cellulose, chitin, and chitosan nanomaterials suitable for fruit preservation. *Carbohydrate Polymers, 259*, Article 117764.
Sun, X., Wu, Q., Zhang, X., Ren, S., Lei, T., Li, W., Xu, G., & Zhang, Q. (2018). Nanocellulose films with combined cellulose nanofibers and nanocrystals: tailored thermal, optical and mechanical properties. *Cellulose, 25*, 1103–1115.
Supian, M. A. F., Amin, K. N. M., Jamari, S. S., & Mohamad, S. (2020). Production of cellulose nanofiber (CNF) from empty fruit bunch (EFB) via mechanical method. *Journal of Environmental Chemical Engineering, 8*, Article 103024.
Tun, T. Z., Nurlatifah, A. T. Htwe, Than, N. N., Khine, M. M., Chavanich, S., Viyakarn, V., Isobe, A., & Nakata, H. (2023). Polymer types and additive concentrations in single-use plastic products collected from Indonesia, Japan, Myanmar, and Thailand. *Science of the Total Environment, 889*, Article 163983.
Turbak, A. F., Snyder, F. W., & Sandberg, K. R. (1983). Microfibrillated cellulose, a new cellulose product: properties, uses, and commercial potential. *ITT Rayonier Inc*. Shelton, WA.
Ueda, T., Ishigami, A., Thumsorn, S., Kurose, T., Kobayashi, Y., & Ito, H. (2022). Structural, rheological, and mechanical properties of polyvinyl alcohol composites reinforced with cellulose nanofiber treated by ultrahigh-pressure homogenizer. *Materials Today Communications, 33*, Article 104316.
Ulbrich, M., & Flöter, E. (2014). Impact of high pressure homogenization modification of a cellulose based fiber product on water binding properties. *Food Hydrocoll, 41*, 281–289.
UNEP, United nations environment programme finance initiative: Beat plastic pollution, (2022).
UNEP. (2024). *Food Waste Index Report 2024. Think Eat Save: Tracking Progress to Halve Global Food Waste., United Nations Environment Programme*.
University of Maine. (2017). *Cellulose nanofibers (CNF) Product Specification*. Process Development Center, University of Maine.
University of Maine, Cellulose nanofibril safety data sheet, process development center, university of maine, 2017.
Usenko, S., Subedi, B., Aguilar, L., & Robinson, E. (2013). Chapter 6 - high-throughput analysis of PPCPs, PCDD/Fs, and PCBs in biological matrices using GC–MS/MS. In

I. Ferrer, & E. M. Thurman (Eds.), *Comprehensive Analytical Chemistry* (pp. 143–158). Elsevier.
Van Nguyen, S., Nguyen, T. K., & Lee, B.-K. (2024). Thermal and heat-sealing properties of polyvinyl alcohol/cellulose nanocrystals-based nanocomposites for food packaging. *Materials Today Communications, 40*, Article 109926.
Vasconcellos, V. M., & Farinas, C. S. (2018). The effect drying process properties of bacterial cellulose films from gluconacetobacter hansenii. *Chemical Engineering Transactions, 64*, 145–150.
Verghese, K., Lewis, H., Lockrey, S., & Williams, H. (2015). Packaging's role in minimizing food loss and waste across the supply chain. *Packaging Technology and Science, 28*, 603–620.
Wang, B., Li, D., Wang, L.-J., Chiu, Y. L., Chen, X. D., & Mao, Z.-H. (2008). Effect of high-pressure homogenization on the structure and thermal properties of maize starch. *Journal of Food Engineering, 87*, 436–444.
Wang, J., Gardner, D. J., Stark, N. M., Bousfield, D. W., Tajvidi, M., & Cai, Z. (2018). Moisture and oxygen barrier properties of cellulose nanomaterial-based films. *ACS Sustainable Chemistry & Engineering, 6*, 49–70.
Wang, L., Chen, C., Wang, J., Gardner, D. J., & Tajvidi, M. (2020). Cellulose nanofibrils versus cellulose nanocrystals: Comparison of performance in flexible multilayer films for packaging applications. *Food Packaging and Shelf Life, 23*, Article 100464.
Wang, L., Li, K., Copenhaver, K., Mackay, S., Lamm, M. E., Zhao, X., Dixon, B., Wang, J., Han, Y., Neivandt, D., Johnson, D. A., Walker, C. C., Ozcan, S., & Gardner, D. J. (2021). Review on nonconventional fibrillation methods of producing cellulose nanofibrils and their applications. *Biomacromolecules, 22*, 4037–4059.
Wang, Q., Du, H., Zhang, F., Zhang, Y., Wu, M., Yu, G., Liu, C., Li, B., & Peng, H. (2018). Flexible cellulose nanopaper with high wet tensile strength, high toughness and tunable ultraviolet blocking ability fabricated from tobacco stalk via a sustainable method. *Journal of Materials Chemistry A: Materials for Energy and Sustainability, 6*, 13021–13030.
Wang, T., & Drzal, L. T. (2012). Cellulose-nanofiber-reinforced poly(lactic acid) composites prepared by a water-based approach. *ACS Appl Mater Interfaces, 4*, 5079–5085.
Woch, J., Małachowska, E., Korasiak, K., Lipkiewicz, A., Dubowik, M., Chrobak, J., Iłowska, J., & Przybysz, P. (2022). Barrier dispersion-based coatings containing natural and paraffin waxes. *Molecules (Basel, Switzerland), 27*.
World Packaging Organisation, Position paper-market trends and developments, (2008).
Xia, J., Zhang, Z., Liu, W., Li, V. C. F., Cao, Y., Zhang, W., & Deng, Y. (2018). Highly transparent 100% cellulose nanofibril films with extremely high oxygen barriers in high relative humidity. *Cellulose, 25*, 4057–4066.
Xu, J., Sagnelli, D., Faisal, M., Perzon, A., Taresco, V., Mais, M., Giosafatto, C. V. L., Hebelstrup, K. H., Ulvskov, P., Jørgensen, B., Chen, L., Howdle, S. M., & Blennow, A. (2021). Amylose/cellulose nanofiber composites for all-natural, fully biodegradable and flexible bioplastics. *Carbohydrate Polymers, 253*, Article 117277.
Xu, S., Girouard, N., Schueneman, G., Shofner, M. L., & Meredith, J. C. (2013). Mechanical and thermal properties of waterborne epoxy composites containing cellulose nanocrystals. *Polymer, 54*, 6589–6598.
Xu, Y., Yang, S., Zhao, P., Wu, M., Song, X., & Ragauskas, A. J. (2021). Effect of endoglucanase and high-pressure homogenization post-treatments on mechanically grinded cellulose nanofibrils and their film performance. *Carbohydrate Polymers, 253*, Article 117253.
Xue, Y., Qi, L., Lin, Z., Yang, G., He, M., & Chen, J. (2021). High-strength regenerated cellulose fiber reinforced with cellulose nanofibril and nanosilica. *Nanomaterials (Basel), 11*.
Yang, B., Zhang, M., Lu, Z., Tan, J., Luo, J., Song, S., Ding, X., Wang, L., Lu, P., & Zhang, Q. (2019). Comparative study of aramid nanofiber (ANF) and cellulose nanofiber (CNF). *Carbohydrate Polymers, 208*, 372–381.
Yano, H., Omura, H., Honma, Y., Okumura, H., Sano, H., & Nakatsubo, F. (2018). Designing cellulose nanofiber surface for high density polyethylene reinforcement. *Cellulose, 25*, 3351–3362.
Yu, W., Cui, J., Zhao, S., Feng, L., Wang, Y., Liu, J., & Zheng, J. (2021). Effects of high-pressure homogenization on pectin structure and cloud stability of not-from-concentrate orange juice. *Frontiers in Nutrition, 8*, Article 647748.
Zhao, G., Du, J., Chen, W., Pan, M., & Chen, D. (2019). Preparation and thermostability of cellulose nanocrystals and nanofibrils from two sources of biomass: rice straw and poplar wood. *Cellulose, 26*, 8625–8643.
Zhao, J., Zhang, W., Zhang, X., Zhang, X., Lu, C., & Deng, Y. (2013). Extraction of cellulose nanofibrils from dry softwood pulp using high shear homogenization. *Carbohydrate Polymers, 97*, 695–702.
Zhou, G., Xu, C., Cheng, W., Zhang, Q., & Nie, W. (2015). Effects of oxygen element and oxygen-containing functional groups on surface wettability of coal dust with various metamorphic degrees based on XPS experiment. *Journal of Analytical Methods, 2015*, Article 467242.
Zhou, Y., Saito, T., Bergström, L., & Isogai, A. (2018). Acid-free preparation of cellulose nanocrystals by TEMPO oxidation and subsequent cavitation. *Biomacromolecules, 19*, 633–639.
Żołek-Tryznowska, Z., Bednarczyk, E., Tryznowski, M., & Kobiela, T. (2023). A comparative investigation of the surface properties of corn-starch-microfibrillated cellulose composite films. *Materials, 16*.
Zuppolini, S., Salama, A., Cruz-Maya, I., Guarino, V., & Borriello, A. (2022). Cellulose amphiphilic materials: Chemistry, process and applications. *Pharmaceutics, 14*, 386.